

Dark Matter Candidates of a Very Low Mass

Kathryn M. Zurek

We review dark matter (DM) candidates of a very low mass, appearing in the window below the traditional weakly-interacting massive particle $m_\chi \lesssim 10$ GeV and extending down to $m_\chi \gtrsim 1$ meV, somewhat below the mass limit where DM becomes wavelike. Such candidates are motivated by hidden sectors such as Hidden Valleys, which feature hidden forces and rich dynamics, but have evaded traditional collider searches looking for New Physics because of their relatively weak coupling to the Standard Model. Such sectors can still be detected through dedicated low-energy colliders which, through their intense beams, can have sensitivity to smaller couplings, or through astrophysical observations of the evolution of DM halos and stellar structures which, through the Universe's epochs, can be sensitive to small DM interactions. We also consider mechanisms where the DM abundance is fixed through the interaction with the SM, which directly motivates the search for light DM in terrestrial experiments. The bulk of this review is dedicated to the new ideas that have been proposed for directly detecting such DM candidates of a low mass, through nuclear recoils, electronic excitations, or collective modes such as phonons and magnons. The rich tapestry of materials and modes in the Condensed Matter landscape is reviewed, along with specific prospects for detection.

CONTENTS

I. Hidden Sector Dark Matter—An Introduction	3
II. Models of Light Dark Matter: a Brief Overview	6
III. Mechanisms for Light Dark Matter Relic Abundance	8
A. Simplified Models in Direct Detection	9
B. Thermal Freeze-out of symmetric and asymmetric dark matter	10
C. Freeze-in	14
D. Strongly Interacting Massive Particles and Elastically-Decoupling Relics	15
IV. Astrophysical, Cosmological and Collider Probes	16
A. Big Bang Nucleosynthesis	16
B. Cosmic Microwave Background	17
C. Large Scale Structure	18
D. Stellar Evolution and Cooling	20
E. Collider Probes of Light Hidden Sectors	20
V. Direct detection of light particle dark matter	22
A. Targets and Excitations for Dark Matter Interactions	23
B. Quantum Mechanics of Dark Matter Scattering	25
1. Example: Spin-Independent Scattering	26
C. In-medium Effects	33
VI. Generalized Dark Matter Interactions	34
A. Effective Field Theory of Dark Matter Scattering with Collective Excitations	34
B. Target Response to Dark Matter Absorption	37
VII. Conclusions	40
Acknowledgments	40
References	40

I. HIDDEN SECTOR DARK MATTER—AN INTRODUCTION

In the search for DM candidates, there are a few considerations that enter, most notably that any DM candidate must satisfy observational evidence. This begins with the observed DM density, which is fixed most precisely at the epoch of the Cosmic Microwave Background (CMB, when the Universe is approximately 380,000 years old, at a redshift $z \sim 10^3 - 10^4$). From that epoch until today, it is known—on the largest scales of the Universe—from the formation of galaxies and clusters of galaxies, as well as galactic rotation curves—that DM density ρ must dilute with the expanding volume of the Universe $\rho = \rho^0(1+z)^3$ (with ρ^0 the density today) and must have very weak interactions with the baryons (so as not to disturb CMB baryon acoustic oscillations), and also with itself so that the structure of galaxies remains approximately oblate (neither a perfect sphere nor a disk). That is, *on average*, the DM must have a cold equation of state ($w = 0$) at least since the Universe is approximately 380,000 years old, and have weak enough interactions with itself and the ordinary matter that the gravitational force dominates the formation of bound structures, and not other forces like baryonic pressure. Beyond this broad set of facts, little is known about the DM. For a classic review of the evidence for DM, see *e.g.* Ref. [1].

Around the time that these facts about the Universe were coming to be broadly accepted (in the '80s) particle physics was itself struggling with some puzzles mostly having to do with questions of “naturalness.” It turned out that solving these problems of naturalness in the Standard Model (SM) of Particle Physics naturally produced two DM candidates. The first of these candidates is the weakly-interacting massive particle (WIMP), which appears as part of the solution to the question of why the Higgs mass (and hence weak forces) are so light; by extension the WIMP mass is typically at the weak scale and they have weak interactions, making them very susceptible to detection with the barrage of experiments probing the weak scale. The second of these candidates is the axion, a possible solution to the question of why there is so little CP violation in the strong interactions. The axion has interactions that are much weaker than weak (corresponding to a mass scale of 10^9 GeV up to the Planck scale), but its much lower mass, and hence much higher number density, gives a boost to the detection probability, typically in cavities that exploit the coherent enhancement of a wave-like state such as axion DM. Both WIMPs and axions can be produced in the early Universe

(thermally and non-thermally, respectively) in an abundance consistent with observations. Multiple experimental efforts are underway to search for these DM candidates. Because they are part of the solution to the SM’s problems, they have interactions with the SM that allow one to predict detection in a sufficiently sensitive device with ordinary particles. Well-defined predictions are appealing to the intrepid DM hunter. See the recent reviews Refs. [2, 3] that describe these ongoing efforts.

However, this narrow focus on these two candidates is despite the fact that, from an observational point of view, a huge mass range of DM particles and an almost as large range of interactions, is observationally possible. On the low mass end, DM can be as light as is consistent with the formation of structure on dwarf-galaxy scales, which implies that the de Broglie wavelength of the DM must be shorter than a typical dwarf galaxy size, implying $m_\chi \gtrsim 10^{-22}$ eV. On the upper mass end, DM is not observed to be clumpy (or grainy) in measurements of the Lyman- α forest; this implies that DM should have mass $m_\chi \lesssim 10^3 M_\odot$ (for reference $1 M_\odot \sim 10^{57}$ GeV) to be sufficiently smooth (see Ref. [4] where shot noise fluctuations from primordial black-hole DM were considered). Any mass in-between is consistent with observations.

Once one releases the requirement that the DM solve one of the Standard Model’s problems, a hidden world of possibilities opens, only subject to the requirement that the DM

- have the observed abundance;
- dilute as a cold non-relativistic state after the CMB epoch;
- have its interactions on large scales be dominated by gravity;
- satisfy the requirement that DM-baryon interactions not damp baryons after the CMB epoch, and not affect the formation of nuclei in the early Universe.

In fact, there is not even a requirement that the Hidden World have only one dark state, have self-interactions much weaker than baryonic, and that *all* of the Dark Sector be non-relativistic.

The structure of a hidden sector (alternatively known as a “hidden valley” or “dark sector”) is shown schematically in Fig. 1. The barrier in between the Standard Model and the hidden sector represents the interaction between the two sectors, with a higher barrier

representing a weaker interaction. The highest barrier is the weakest force of all, gravity. In order to detect DM through individual particle interactions with the SM, there must be other, much lower, barriers, represented as lower peaks. The mass scale of the hidden sector, represented by the height of the “floor,” is unknown.

One is tempted to become overwhelmed by such a huge mass range of DM, types of dark sectors and their interactions. Thus, it helps to break it down according to the physics governing the DM masses and interactions. In this article, we will focus on a mass range of particle DM that is motivated, by its relic abundance, to have large enough interactions with the SM to be detectable through particle interactions. When the DM is heavier than approximately 10 TeV, setting its relic abundance through interactions with the SM is challenging (as we will see explicitly below). While there are exceptions, when the DM mass is much heavier than the electroweak scale, detection through SM interactions is generally not motivated by abundance. For heavier mass DM, one can use gravitational means (*e.g.* pulsar timing [5] or the unique motions of stars [6]) or additional DM-SM fifth force to search for such candidates [7], often through astrophysical means. On the other end of the mass scale, when the DM is lighter than ~ 1 eV, DM behaves like a wave rather than an individual particle. Detection techniques in this “ultralight” mass regime focus on utilizing coherence, often in cavities or with other AMO techniques [8]. While this is a vibrant area of research, it will not be the focus of this article.

We will focus on hidden sector DM candidates in the “low mass” range, whose relic abundance is still naturally set by its interactions with the SM, where it is motivated to search for such a state through detection of individual particles in terrestrial experiments. This implies a DM mass range between approximately a few keV (below which DM which is produced by its particle interactions with the SM will be too warm to cluster appropriately, see *e.g.* Ref. [9]) and approximately 10 GeV, just below the weak scale. Because these Hidden Sector states have a mass below the weak scale interactions, making for a low mass floor in the schematic of Fig. 1, we refer to these DM models as Hidden Valley (HV) or Hidden Sector (HS) DM.

The outline of the rest of this review is as follows. In the next Section, we review how DM candidates of a very low mass can naturally have their relic abundance set through interactions with the SM. We characterize the various kinds of mechanisms that are often

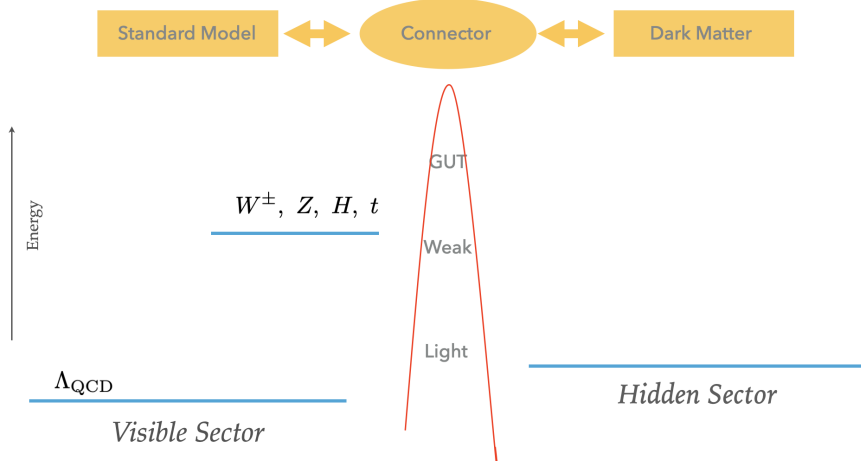


Figure 1. Schematic of Hidden Sector Dark Matter. The barrier in the center of the figure represents the interaction (from a grand unified theory (GUT), weak scale or light mediators) between the two sectors, with a higher barrier representing a weaker interaction. The mediator connects the visible and hidden sector, where the height of the floor in the two sectors represents the mass gap. In the visible sector we have the standard model, with a mass gap for the baryons of around a GeV, while in the DM sector, it is unknown the scale of the mass gap, or the structure of the states there.

utilized in the literature to set the relic abundance. We then turn to examining astrophysical and cosmological probes for HVDM, which by itself sheds a light on where DM might be detected in terrestrial experiments. Then we turn to the main focus of the article: terrestrial probes for HVDM, focusing mostly on direct detection experiments. Novel probes must be invented to search for HVDM, because the traditional nuclear recoil probes of WIMP DM are ineffective; more specifically, this implies utilizing the wealth of “collective modes” (such as phonons and magnons) that are available in Condensed Matter systems. We also briefly review other kinds of terrestrial probes for HVDM, such as accelerator based experiments.

II. MODELS OF LIGHT DARK MATTER: A BRIEF OVERVIEW

There are a broad range of Hidden Sector models, necessitating a strong selection of theory for this review. We will focus on direct detection prospects in terrestrial experiments, and therefore on interactions with the SM that could be detected. These interactions are most motivated when they also set the relic abundance, as we discuss in the next section.

In the dark sector itself, the structure is relatively unconstrained, especially if the mass gap in the hidden sector is $\gtrsim 10$ MeV where constraints from Big Bang Nucleosynthesis (BBN) from a thermalized hidden sector can be most easily satisfied. For example, the hidden sector could be a/an [10, 11]

- QCD-like theory with F -flavors and N -colors, with only light or heavy quarks, or adjoint quarks;
- QED-like theory with no massless photon;
- Pure-gluon theory;
- Remnant from SUSY breaking;
- Partially Higgsed SU(N) theory;
- Seiberg duality cascade;
- Unparticles;
- Sector arising from an Randall-Sundrum or Klebanov-Strassler throat in extra dimensions.

Hidden sectors with such structures will naturally give rise to DM self-interactions. Strongly coupled hidden sectors have weakly coupled duals, so it is also possible to write effective Lagrangians in terms of weakly-coupled scalars, fermions and vector mediators [12]. To take a particularly simple example, the dark sector could be a QCD-like theory with $N = 2$, 2 light flavors, and no heavy flavors [10]. Such a hidden sector has gapped degrees of freedom, hidden pions π_v^\pm , π_v^0 . Note the \pm here does not denote electric charge, but rather charge under a new global symmetry in the hidden sector that stabilizes the pions carrying the global symmetry π_v^\pm . The relic abundance is fixed by

$$\pi_v^+ \pi_v^- \rightarrow \pi_v^0 \pi_v^0, \quad (1)$$

with $\pi_v^0 \rightarrow f \bar{f}$ decaying, for example, to SM fermions to which the dark sector states couple via the connector state. This structure also appears in Secluded DM models [13, 14]. There may also be a mechanism to generate an asymmetry (or chemical potential) between π_v^+ and

its anti-particle, the motivation for theories of hidden-sector Asymmetric Dark Matter [15]. See also Ref. [16] for a discussion of HV/HS DM in the context of asymmetric DM. This general framework triggered a slew of model building, from atomic [17], quirky [18] and glueball [19] DM, to the WIMPless [20] and SIMP [21] miracles.

Hidden sectors also naturally allow for “portals” between the two sectors, through which the DM interacts with the SM, giving rise to signatures in terrestrial experiments. Since the DM is electrically neutral, there are two natural portals involving dimension-4 operators

- Vector Portal including a kinetically mixed dark photon [22] (Ref. [23] for an application to DM)

$$\mathcal{L}_{A'} \supset -\frac{1}{2}m_{A'}^2 - \frac{1}{4}F'^{\mu\nu}F'_{\mu\nu} - \frac{\epsilon}{2}F_{\mu\nu}F'^{\mu\nu} - y_\chi A'_\mu \bar{\chi}\gamma^\mu\chi. \quad (2)$$

The vector mediator can also, for example, be a gauge boson from a $B - L$ symmetry, U_{B-L} [24].

- Scalar Portal including via Higgs mixing [11, 25],

$$\mathcal{L}_{H\phi} \supset -\frac{1}{2}m_\phi^2|\phi|^2 - \kappa|H|^2|\phi|^2. \quad (3)$$

One can also have a hadrophilic or leptophilic scalar, as discussed in detail in Ref. [24].

Another important feature in the hidden sector, besides its self-interactions and the portal to the visible sector, is the mass gap fixing m_χ . While by no means necessary, the theory becomes more predictive if this gap is fixed by a relation with the visible sector. This can happen, for example, if the confinement scale in the hidden sector is triggered by visible sector confinement [26], or if supersymmetry breaking in the visible sector triggers supersymmetry breaking in the hidden sector and fixes the mass scales in that sector [27]. While we do not go into details of these models in this review, the mechanism that generates the mass gap in the hidden sector can also give rise to predictive interaction rates in terrestrial experiments. We explore some of these cases in the next two sections.

III. MECHANISMS FOR LIGHT DARK MATTER RELIC ABUNDANCE

The direct search for DM candidates whose mass is below the electroweak scale depends on the DM having couplings to the SM other than gravitational. The strength of those

couplings, and in particular whether they are large enough to give rise to detectable signals in terrestrial experiments, is best motivated if the DM relic abundance is fixed through its interactions with the SM. We review here mechanisms for setting the relic abundance, with the goal of showing how such DM candidates could be observed through a scattering or absorption process in a direct detection experiment.

A. Simplified Models in Direct Detection

Eqs. 2, 3 comprise simplified models of portals mediating interactions with the SM, with m_ϕ or $m_{A'}$ denoted more generally as mediators with mass m_M . It is often useful to employ simplified models as a general framework for understanding how relic abundance considerations interplay with astrophysical, cosmological and direct detection constraints. A typical interaction cross-section of DM with coupling $\alpha_\chi = \frac{g_\chi^2}{4\pi}$ via a mediator, on a target T having a coupling $\alpha_T = g_T^2/4\pi$, takes the form

$$\bar{\sigma}_T = \frac{16\pi\alpha_T\alpha_\chi}{(m_M^2 + \mathbf{q}_0^2)^2}\mu_{T\chi}^2 \quad (4)$$

in a direct detection experiment, where $\mu_{T\chi}$ is the target-DM reduced mass, and \mathbf{q}_0 is a typical momentum transfer in the experiment, used here for defining the reference cross-section. For electron targets, the reference momentum is taken to be $q_0 = \alpha m_e$. The same product of couplings, $\alpha_T\alpha_\chi$ typically sets the relic abundance of DM in models where DM is produced through its interaction with the SM. In the case of scattering via a heavy vector mediator, on an electron target lighter than the DM, the direct detection cross-section can be written as

$$\bar{\sigma}_e = \frac{16\pi\alpha_e m_e^2}{m_\chi^4} y_{RA}, \quad (5)$$

where we have separated a relic-abundance parameter y_{RA}

$$y_{RA} \equiv \alpha_\chi \left(\frac{m_\chi}{m_{A'}} \right)^4. \quad (6)$$

A summary plot showing the proposed reach in $\bar{\sigma}_e$ of several direct detection experiments as a function of light DM mass is shown in Fig. 2. In the rest of the review, one goal will be to illuminate how the various reach curves and constraints are computed. The orange

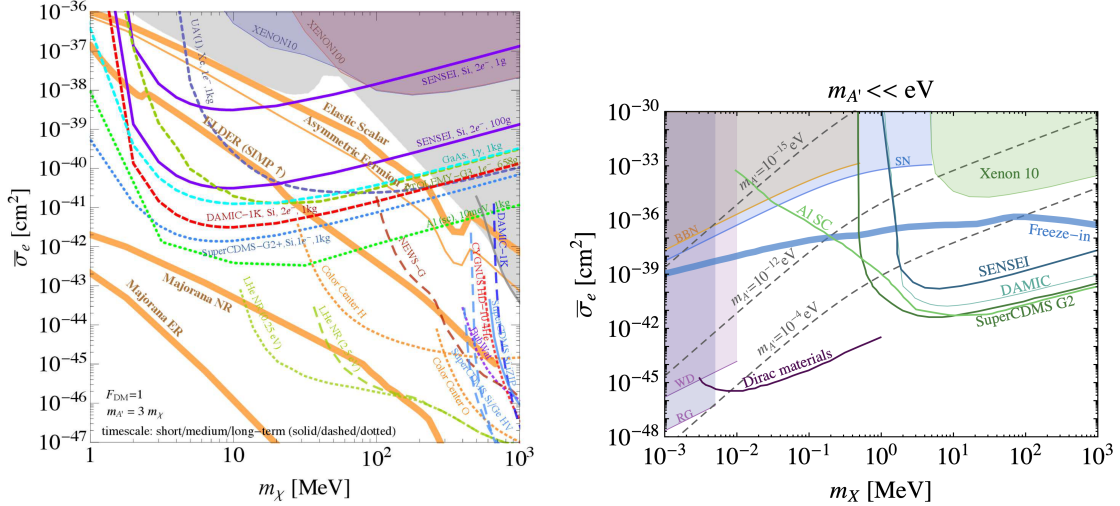


Figure 2. Direct Detection reach spaces for *left*: a massive vector mediator coupled to electrons (figure from Ref. [8]), and *right*: a massless dark photon (figure from Ref. [24]). Both panels show benchmarks, as orange or blue bands in each figure, where the same couplings that fix the relic abundance also give rise to the direct detection interaction, motivating laboratory searches. This occurs, for example, for p -wave freeze-out of scalar DM (see discussion around Eq. 12), Asymmetric DM (see discussion around Eq. 17), Freeze-in (Eq. 22), and SIMPs/ELDERs (Eq. 26). The various ideas to directly detect light DM, such as through a silicon or germanium target, through superconductors, or via polar materials, will be discussed in subsequent subsections. We also discuss stellar cooling bounds, such as from red giants (RG), white dwarves (WD), and supernovae (SN).

bands in the left plot and the blue band in the right plot correspond to the regions of model space where the DM abundance in the Universe is fixed by the same couplings that give rise to the scattering in direct detection experiments. We now turn to discussing concretely how the scattering cross-section in direction detection experiments can be related to the relic abundance in three common cases that set benchmarks in terrestrial searches for light DM.

B. Thermal Freeze-out of symmetric and asymmetric dark matter

Thermal freeze-out occurs when the temperature drops below the DM mass, and the equilibrium process, $\chi\bar{\chi} \leftrightarrow f\bar{f}$, becomes simply an annihilation process:

$$\chi\bar{\chi} \rightarrow f\bar{f}. \quad (7)$$

Freeze-out fixes the relic abundance to a value obtained by solving a Boltzmann equation

$$\frac{dY_{\pm}}{dx} = -\frac{x\langle\sigma v\rangle s}{H(m_{\chi})}(Y_+Y_- - (Y^{eq})^2), \quad (8)$$

where we are allowing DM to have separate number densities for particle and antiparticle to allow for a DM asymmetry: $Y_{\pm} = n_{\pm}/s$, where s is the entropy density. Here $x = m_{\chi}/T$, the Hubble parameter $H(m_{\chi})$ is evaluated at $T = m_{\chi}$ in a radiation-dominated universe, and $Y^{eq} \simeq ax^{3/2}e^{-x}$ is the equilibrium number density, with a dependent on the number of thermalized degrees of freedom. The annihilation cross-section is parameterized as s -wave ($n = 0$) or p -wave ($n = 1$): $\langle\sigma v\rangle \equiv \sigma_0(T/m)^n = \sigma_0x^{-n}$, where $\frac{3}{2}T = \frac{1}{2}m\langle v^2\rangle$. Note that for p -wave interactions, since the DM velocity drops as the Universe cools, the interaction rate is much smaller in the late than early Universe. This can be important for observational constraints, such as on the annihilation cross-section from the CMB relative to the freeze-out cross-section. In the case where there is no DM particle-anti-particle asymmetry, freeze-out occurs when $n_{\chi}\langle\sigma_A|v\rangle \simeq H(x_f)$, and one can do a back-of-the-envelope calculation of the needed annihilation cross-section to fix the observed relic abundance ρ_{χ}^0 :

$$\begin{aligned} \langle\sigma v\rangle &\sim \frac{T_f^2}{M_{pl}} \frac{m_{\chi}}{\rho_{\chi}(T_f)} \\ &= \frac{T_f^2}{M_{pl}} \frac{m_{\chi} T_0^3}{\rho_{\chi}^0 T_f^3} \\ &= \frac{T_0^3}{M_{pl}} \frac{x_f}{\rho_{\chi}^0} \\ &\simeq 3 \times 10^{-26} \text{ cm}^3/\text{s} \left(\frac{x_f}{20}\right), \end{aligned} \quad (9)$$

where $x_f \simeq 20$ is the freeze-out temperature obtained from solving the Boltzmann equation for s -wave annihilation and DM in the WIMP window $m_{\chi} \simeq 1$ TeV. It has only logarithmic sensitivity to the DM mass and parameter n , but we quote its value below for general particle asymmetries. An s -wave annihilation process to a light vector particle scales parametrically as

$$\langle\sigma v\rangle \simeq \frac{\pi\alpha_{\chi}^2}{m_{\chi}^2} \sqrt{1 - \left(\frac{m_M}{m_{\chi}}\right)^2} \simeq 3 \times 10^{-26} \frac{\text{cm}^3}{\text{s}} \left(\frac{g_{\chi}}{0.4}\right)^4 \left(\frac{2 \text{ TeV}}{m_{\chi}}\right)^2, \quad (10)$$

where we have taken the vector force mass to be much smaller than the DM mass, $m_M \ll m_{\chi}$. That $g_{\chi} \sim 1$ when $m_{\chi} \sim 1$ TeV is parametrically the reason that weak scale DM is

said to be motivated by thermal freeze-out, known colloquially as “the WIMP miracle.” One can see immediately that the DM cannot be pushed much heavier than ~ 10 TeV without running into a regime where couplings become non-perturbative and the theory is inconsistent. However, as DM becomes lighter, one simply needs to scale down the coupling product α_χ linearly with m_χ to satisfy the same relic abundance considerations. Thus hidden sector DM of a low mass is equally well motivated by thermal freeze-out considerations.

More generally, for an s -channel annihilation process to electrons through a mediator, vector or scalar, the annihilation cross-sections at freeze-out are

$$\langle\sigma v\rangle_V \simeq \frac{16\pi\alpha_\chi\alpha_e m_\chi^2}{(4m_\chi^2 - m_{A'}^2)^2} \quad \text{and} \quad \langle\sigma v\rangle_S \simeq \frac{2\pi\alpha_\chi\alpha_e m_\chi^2}{(4m_\chi^2 - m_S^2)^2} \frac{1}{x_f}. \quad (11)$$

As DM drops below approximately 10 GeV down to $2m_e$, its relic number density remains high enough that s -wave annihilation to SM states, *in the absence of a particle-anti-particle asymmetry*, during the CMB epoch is ruled out, see Refs. [28–31] and discussion in Sec. IV B. The basic reason for the CMB constraint is that the energy released in DM annihilation can distort the surface of last scattering, placing a lower bound on the DM mass. This can be ameliorated through p -wave annihilation (which occurs if fermionic DM annihilates through a scalar mediator, or if scalar DM annihilates through a vector boson as was proposed for MeV DM, see Refs. [12, 32, 33]). In this case, the annihilation rate is suppressed by the velocity of the DM in the late Universe (in the Milky Way, $v \sim 10^{-3}$, while for the smooth background $v \sim \sqrt{T/m_\chi}$), while in the early Universe (at freeze-out, the velocity is $v \sim \frac{1}{3}$) the rate is similar to the s -wave case. For the s -wave case, one finds the relic abundance parameter in Eq. 6 which enters into the direct-detection cross-section Eq. 5

$$y_{\text{RA}} \simeq 10^{-11} \left(\frac{m_\chi}{10 \text{ MeV}}\right)^2 \left(\frac{x_f}{20}\right) \left(1 - \frac{4m_\chi^2}{m_{A'}^2}\right)^2. \quad (12)$$

For the case of p -wave annihilation through a scalar mediator, the couplings must be correspondingly (somewhat) larger to compensate the v^2 suppression. The model space of p -wave annihilating scalar DM is shown as the orange band “Elastic scalar” in the left panel of Fig. 2.

The CMB bounds on light DM annihilation can also be satisfied if DM has a particle-anti-particle asymmetry [30], as discussed below in Sec. IV B. Asymmetric DM has its relic abundance fixed via a chemical potential, similar to the particle-anti-particle asymmetry in

the visible sector (see Ref. [15] for a review). However, the particle-anti-particle asymmetry of asymmetric DM only becomes visible if the symmetric abundance is efficiently removed through annihilation in the early Universe. This is similar to baryons and leptons in the SM, which efficiently annihilate through, *e.g.*, $e^+e^- \rightarrow \gamma\gamma$ and $p\bar{p} \rightarrow \pi^+\pi^-$. In the SM, these processes are highly efficient, such that positrons and anti-protons and neutrons are extremely rare in the Universe, except if they are produced in astrophysical accelerators that generate cosmic rays. For Asymmetric DM to satisfy bounds on DM annihilation rates at the CMB epoch, the particle-anti-particle annihilation rate must have been *large enough* to effectively remove the anti-particle, placing a *lower* bound on the annihilation cross-section. This in turn will place a lower bound on the scattering cross-section via Eq. 5 which also serves as a benchmark for light DM direct detection experiments. We will briefly summarize the treatment in Ref. [30] relevant for our purposes. Solving the Boltzmann equation for a general particle-anti-particle asymmetry gives rise to the late-time ratio of particle to anti-particle asymmetries [30, 34]:

$$r_\infty \equiv \frac{Y_-}{Y_+}(\infty) \simeq \frac{Y_-(x_f)}{Y_+(x_f)} \exp\left(\frac{-\eta_\chi \lambda \sqrt{g_*}}{x_f^{n+1}(n+1)}\right), \quad (13)$$

where $\eta_\chi \equiv Y_\chi - Y_{\bar{\chi}}$ and $\lambda \equiv 0.265 M_{pl} m_\chi \sigma_0$. It turns out that numerically one can set $r(x_f) \sim 1$ to obtain r_∞ . The required annihilation cross-section to achieve a particle symmetric component r_∞ ($r_\infty \ll 1$ corresponds to a large asymmetry) is thus

$$\langle\sigma v\rangle \simeq c_f \times 5 \times 10^{-26} \text{ cm}^3/\text{s} \times \ln\left(\frac{1}{r_\infty}\right), \quad (14)$$

where $c_f \equiv \left(\frac{x_f}{20}\right) \left(\frac{4}{\sqrt{g_{*,f}}}\right)$. One can combine this with the bound on the annihilation cross-section from the CMB [28–31]

$$\langle\sigma v\rangle_{\text{CMB}} \lesssim \frac{10^{-27} \text{ cm}^3/\text{s}}{f} \left(\frac{m_\chi}{1 \text{ GeV}}\right) \left(\frac{1}{r_\infty}\right) \quad (15)$$

to obtain an upper bound on r_∞ :

$$r_\infty \ln\left(\frac{1}{r_\infty}\right) \lesssim \frac{0.02}{f c_f} \left(\frac{m_\chi}{1 \text{ GeV}}\right), \quad (16)$$

where f parameterizes an ionizing efficiency ($f \sim 1$ for annihilation to charged leptons, but is smaller for annihilation to hadronic states). This corresponds to a *lower* bound on the

s -wave annihilation $\langle\sigma v\rangle_{\text{CMB}} = \langle\sigma v\rangle_V$ [30]:

$$\langle\sigma v\rangle \gtrsim 5c_f \times 10^{-26} \frac{\text{cm}^3}{\text{s}} \left(\ln \left(40f c_f \times \frac{1 \text{ GeV}}{m_\chi} \right) + \ln \ln \left(40f c_f \frac{1 \text{ GeV}}{m_\chi} \right) \right). \quad (17)$$

This s -wave annihilation cross-section is a factor of several larger than what is required to fix the relic abundance in the symmetric s -wave case, in order to achieve a sufficient depletion of the symmetric relic abundance (see Fig. 2 of Ref. [30]). The CMB bound thus gives rise to a scattering cross-section for the ‘‘Asymmetric Fermion’’ in Fig. 2:

$$\sigma_e \gtrsim 4 \times 10^{-39} \text{ cm}^2 \left(\frac{10 \text{ MeV}}{m_\chi} \right)^2 \left(\frac{\mu_{e\chi}}{0.5 \text{ MeV}} \right)^2 \ln \left(\frac{40 \text{ GeV}}{m_\chi} \right) \frac{(4m_\chi^2 - m_M^2)^2}{m_M^4}, \quad (18)$$

which is derived by combining Eqs. 4, 11, 17 for the vector mediator. On the line in Fig. 2, there is an arrow upward to indicate that the CMB bound demands *minimum* couplings to remove the symmetric abundance. An elastic scalar DM line is found nearby on the same panel, since this case requires similar, but slightly larger, couplings.

C. Freeze-in

Freeze-in is a process that dominantly occurs at low temperatures, if the DM is not in equilibrium with the SM [35]. An initially unpopulated DM state is gradually populated through *occasional* annihilations of SM states to DM. For example, if DM is lighter than the pion mass, the dominant freeze-in process is via electrons or plasmons γ^*

$$e^+e^- \rightarrow \chi\bar{\chi}, \quad \gamma^* \rightarrow \chi\bar{\chi}. \quad (19)$$

For the purposes of the estimate here, we focus on the first process, though the second process impacts the expected scattering rate in direct detection by up to a factor of ten for $m_\chi \sim \text{keV}$, while having little impact for $m_\chi \sim \text{MeV}$ [36]. In the case that the DM is not initially in thermal equilibrium, the Boltzmann equation becomes

$$\frac{dY}{dT} = -\frac{\langle\sigma|v\rangle}{HTs} n^2. \quad (20)$$

If we take $\langle\sigma|v\rangle \sim \frac{g_\chi^2 g_e^2}{4\pi T^2}$ as expected for infrared dominated effects, one finds [36, 37]

$$Y \sim 10^{-4} \frac{g_\chi^2 g_e^2 M_{\text{Pl}}}{T}. \quad (21)$$

Taking $T \sim 1$ MeV, where the electrons themselves drop out of thermal equilibrium, and fixing Y by the observed abundance through the relation $\rho_\chi^0 = m_\chi Y s_0$ where s_0 is the entropy density today, then we obtain the approximate scaling

$$g_\chi g_e \sim 10^{-12} \sqrt{\frac{1 \text{ MeV}}{m_\chi}}, \quad (22)$$

where we have used that the number density of DM $Y \propto 1/m_\chi$ in solving for the couplings. For $m_\chi \lesssim m_e$, the direct detection cross-section, using Eq. 4, then scales as

$$\sigma_e \simeq 10^{-39} \text{ cm}^2 \left(\frac{m_\chi}{1 \text{ keV}} \right). \quad (23)$$

This estimate corresponds to the blue curve in the right panel of Fig. 2 for $m_\chi \lesssim 1$ MeV. For $m_\chi \gtrsim m_e$, the freeze-in temperature in Eq. 21 is $T \sim m_\chi$ and the scattering cross-section becomes approximately independent of m_χ . At even higher masses $m_\chi \gtrsim m_\pi$, new processes involving pions enter and we do not estimate this rate here. One can see, however, over much of the mass space, simple estimates allow one to obtain an *approximate* expected interaction cross-section with electrons.

D. Strongly Interacting Massive Particles and Elastically-Decoupling Relics

DM freeze-out can be dominated by $3 \rightarrow 2$ processes [21, 38], with a cross-section parameterized by

$$\langle \sigma_{3 \rightarrow 2} v^2 \rangle \equiv \frac{\alpha^3}{m_\chi^5}. \quad (24)$$

Parametrically α is proportionate to a dark gauge coupling constant $\alpha_D \equiv g_D^2/4\pi$, though here, following [21, 38, 39], α is allowed to absorb $\mathcal{O}(1)$ factors. The observed relic abundance is obtained when

$$\alpha \simeq 0.3 \left(\frac{m_\chi}{10 \text{ MeV}} \right). \quad (25)$$

These processes continually dump kinetic energy into the DM by “cannibalizing” the DM’s rest energy. This is observationally ruled out, since the DM would be much warmer than observed [40, 41]. The solution to this problem, as proposed in Ref. [21, 38], is to have a light mediator which bleeds off the energy into the SM sector continuously, typically via a

kinetic mixing parameter ϵ between a dark and visible photon. In this picture, the elastic scattering process which bleeds off the excess energy decouples after the freeze-out of the $3 \rightarrow 2$ process.

This idea was generalized in Ref. [39, 42] by allowing $3 \rightarrow 2$ processes in the hidden sector, as well as $2 \rightarrow 2$ processes (notably $\chi\bar{\chi} \rightarrow e^+e^-$) as in freeze-out to play a role. Since the $\chi\bar{\chi} \leftrightarrow e^+e^-$ decouples when both directions are in equilibrium, this was called an Elastically Decoupling Relic (ELDER) [39, 42]. Thus, the ELDER smoothly interpolates between the elastic freeze-out case (for large enough kinetic mixing, where the $3 \rightarrow 2$ process freezes-out well before the annihilation to SM) and the SIMP case (where elastic decoupling with the SM occurs before the $3 \rightarrow 2$ process freezes-out). In the ELDER limit, the relic abundance is set dominantly by the decoupling temperature from the SM, which is given by [39]

$$y_{\text{ELDER}} = \epsilon^2 \alpha_D \left(\frac{m_\chi}{m_{A'}} \right)^4 \simeq 6 \times 10^{-15} \left(\frac{g_{*,d}}{10} \right)^{1/2} \left(\frac{m_\chi}{10} \right) \left(\frac{x_d}{17} \right)^6, \quad (26)$$

where ϵ , α_D are defined above and $x_d = m_\chi/T_d$ with T_d the elastic decoupling temperature. This will allow to give a precise benchmark for the ELDER scenario, also indicated by the orange band in the left panel of Fig. 2.

IV. ASTROPHYSICAL, COSMOLOGICAL AND COLLIDER PROBES

When considering whether a DM candidate of a very low mass is detectable in a terrestrial experiment, a wide range of astrophysical, cosmological and collider constraints must be taken into consideration. Here we summarize the main features, but refer the reader to Refs. [16, 24, 30] for a further discussion on the interplay of the constraints with terrestrial observations.

A. Big Bang Nucleosynthesis

Big bang nucleosynthesis is a powerful constraint if DM is lighter than an MeV in mass. Measurements of hydrogen, deuterium and helium, synthesized dominantly when the Universe had a temperature $T_{\text{BBN}} \sim 0.1 - 1$ MeV at a time $t \sim 1$ s indicate that the Universe was expanding at a rate consistent with a relativistic SM photon and three neutrino species. If any other state were in equilibrium with the SM, for example through $\chi\bar{\chi} \leftrightarrow f\bar{f}$ interactions,

this would cause the Universe to expand more quickly, and change the relative abundance of the light elements, parameterized by the effective number of neutrino species N_{eff} . Current data constrains $\Delta N_{\text{eff}}^{\text{BBN}} \lesssim 0.2$ [43, 44], implying a more than 3σ tension with a single real scalar having a temperature similar to that of neutrinos. This implies that any DM candidate with mass $\lesssim 10$ MeV has its couplings to the SM constrained by BBN.

Note that in general, for a DM candidate to be detectable, not only are there the DM degrees-of-freedom, but there is also a mediator that couples the DM to the SM. The mediator must also either (i) be heavier than $\sim 1 - 10$ MeV; or (ii) have sufficiently small couplings to the SM that it remains out of equilibrium; or (iii) contribute $\Delta N_{\text{eff}}^{\text{BBN}} \gtrsim 0.57$ (for a real scalar DM) and be in $\sim 4\sigma$ tension with BBN. This limits the types of DM models that can be detected in terrestrial experiments. See Ref. [24] for an extensive discussion and application to terrestrial experiments and Ref. [43, 44] for updated BBN constraints.

For example BBN constraints are the reason why, for the model space detectable by terrestrial direct detection experiments, DM lighter than an MeV should be mediated by a very light particle, as in the right panel of Fig. 2. Direct detection experiments are sensitive to extremely small couplings via light mediators (as in Eq. 22), because of the direct detection enhancement at low momentum transfers (as in Eq. 4, with $m_M \rightarrow 0$). For such small couplings the hidden sector is not in equilibrium with the visible sector, except at larger couplings, shown as the shaded orange region in the left-hand panel of Fig. 2. Likewise, for DM mediated through a heavier particle (having mass $m_M \gtrsim m_\chi v$, where v is the Milky Way virial velocity), the couplings are much larger (see *e.g.* Eq. 10 for typical freeze-out couplings). In this case, the hidden sector generically comes into equilibrium with the visible sector, such that hidden sectors with mass below a few MeV are already ruled out by BBN; this is one reason the plots in the left-hand panel of Fig. 2 extend only to $m_\chi \gtrsim 1$ MeV.

B. Cosmic Microwave Background

As already discussed in the freeze-out and asymmetric DM section, the CMB places a variety of constraints on a DM candidate of a very low mass. First, the CMB also places a constraint, at 2σ , roughly consistent with the BBN bound, $\Delta N_{\text{eff}}^{\text{CMB}} \lesssim 0.6$. Since the CMB epoch is at a redshift $z \sim 10^3 - 10^4$, while the BBN epoch is at $z \sim 10^{10}$, one cannot simply

assume, if the constraint on additional thermal relativistic species is met at one epoch, that it is met at another epoch. Note that in the future, CMB Stage IV will dramatically improve on this constraint, $\sigma(N_{\text{eff}}^{\text{CMB}}) \approx 0.04$.

In addition, the CMB is very sensitive to any additional ionizing radiation that can be dumped into the photon-baryon bath. For example, the Planck limit on DM energy injection due to annihilation is given by Eq. 17. Since, to set the thermal relic abundance for DM through annihilation, we require $\langle\sigma v\rangle \sim 3 \times 10^{-26} \text{ cm}^3/\text{s}$, this implies that light (sub-GeV) DM cannot have its relic abundance set by s -wave annihilation while remaining consistent with CMB-epoch ionization constraints. There are two ways to circumvent this constraint, as discussed in Sec. III B: p -wave annihilation where the cross section is v suppressed, or asymmetric DM where $r_\infty \ll 1$. As highlighted above, models of asymmetric DM must have an efficient mechanism for removing the symmetric abundance of DM early in the Universe. This implies a *lower* bound on the annihilation cross-section in the early Universe, shown in the left panel of Fig. 2 as the “Asymmetric fermion” curve, to adequately dilute the symmetric abundance.

C. Large Scale Structure

Large scale structure places two important bounds on DM having a very low mass. The first important bound is the warm DM bound, from the formation of structure on small scales, as observed with Lyman- α forest and other large-scale structure measurements of DM clustering [9, 45]. Thermalized DM has a relation between its velocity and temperature given by

$$v = \sqrt{\frac{3T}{m_\chi}}. \quad (27)$$

If DM has its temperature on the same order as the visible temperature $T \sim 10^{-4} \text{ eV}$, and we require DM to be cold enough for it to fall into structures having virial velocity $v \sim 10^{-4}$ (as observed in dwarf galaxies for example), this implies that DM should have mass

$$m_\chi \gtrsim 10 \text{ keV}. \quad (28)$$

This is the back-of-the-envelope estimate of the warm DM bound (which can be more carefully derived simulating the formation of structures with warm DM *e.g.* [9, 45]). DM may

still be lighter than this bound, but its temperature should not be set by the interactions with the SM (as happens, for example with non-thermal mechanisms such as the misalignment mechanism for the axion or inflationary production of vector DM [46, 47]).

If DM has an interaction with the SM through a relatively light gauge boson, this can also cause late kinetic decoupling between the SM and the dark sector, and modify the matter power spectrum on small scales. For example, DM can couple to neutrinos through a mediator (product of couplings to the mediator $g_\chi g_\nu$), giving rise to a kinetic decoupling temperature

$$T_{\text{kd}} \simeq \text{keV} \frac{m_M}{\text{MeV}} \left(\frac{m_\chi}{\text{MeV}} \right)^{1/4} \left(\frac{10^{-6}}{g_\chi g_\nu} \right)^{1/2}. \quad (29)$$

Such a kinetic decoupling temperature is bounded by the Lyman-alpha forest, see Ref. [33].

In addition, DM of a very low mass also tends to come with new light forces that can mediate large self-interactions. The self-interaction rate is bounded by the shape of DM halos, which implies that DM self-interactions should be rare enough that the formation of halos is dominated by gravitational interactions. This implies [48]

$$\frac{\sigma}{m_\chi} \lesssim 0.1 - 10 \text{ cm}^2/\text{g}, \quad (30)$$

where the large range of possible bounded cross-sections is due both to the large range of system mass scales and interaction times (from dwarf galaxies at $10^7 M_\odot$ to clusters of galaxies at $10^{15} M_\odot$), as well as the still-somewhat-imprecise nature of simulations which depend on baryonic effects and their (non-linear) feedback on the DM structure formation process. Especially when the mediator is light, this places severe limits on the DM-mediator coupling (taking $\frac{\sigma}{m_\chi} = 1 \text{ cm}^2/\text{g}$):

$$\alpha_\chi \lesssim 6 \times 10^{-10} \times \left(\frac{m_\chi}{1 \text{ MeV}} \right)^{3/2}. \quad (31)$$

When the mediator becomes massive ($m_\phi > m_\chi v$) we have the less severe limit

$$\alpha_\chi \lesssim 0.025 \left(\frac{1 \text{ keV}}{m_\chi} \right)^{1/2} \left(\frac{m_\phi}{1 \text{ MeV}} \right)^2. \quad (32)$$

See Refs. [49, 50] for further discussion.

D. Stellar Evolution and Cooling

When the DM, or the mediator, is lighter than the temperature of a star, production of dark sector particles can lead to cooling that is more efficient than happens in the standard model, where states are strongly coupled to the stellar plasma; see Ref. [51] for a classic review. This cooling changes the evolution of the star from that predicted by standard theory, and could be observed. This has long been appreciated in particular for axions, but also becomes relevant for DM and mediators with mass $\lesssim 30$ MeV, the temperature of a supernova. In addition to supernovae, Red Giant (RG, relevant for masses $\lesssim 10$ keV), Horizontal Branch (HB, $\lesssim 100$ keV) for nucleon couplings, and White Dwarves (WD, $\lesssim 10$ keV) are all relevant. Constraints from these stellar cooling limits are shown as shaded regions in Fig. 2, as well as in Fig. 3. When the coupling becomes large enough, particularly in dense environments like the neutron stars sitting inside supernovae, trapping becomes relevant. The supernova cooling bounds have recently been updated in Ref. [52], while the RG, HB, WD and stellar cooling bounds, for mediator couplings to nucleons, electrons and dark photons, are quoted in detail in Ref. [24].

Light DM, in particular if it carries a particle-anti-particle asymmetry that prevents annihilation, can accumulate in the center of stars and also cause a change in their evolution. This has been considered in particular for neutron stars, either due to inducing an instability (we refer the reader to the discussion in Ref. [16] for a summary) or kinetic heating [53]. Accumulation of light DM can also lead to modification of main branch stellar evolution [54] and in Brown [55] and White [56, 57] Dwarves. We refer the reader to Ref. [58] for a fairly up-to-date list of references on compact star constraints on hidden sector DM interactions with electrons and nucleons.

E. Collider Probes of Light Hidden Sectors

Intensity experiments, such as beam dumps featuring a large number of protons on target, can probe relatively light (typically sub-GeV mass) hidden sector particles. The constraints are most direct on the mediating particle (vector or scalar), and depend on the decay channel, whether to visible particles (notably e^+e^-) or invisible.

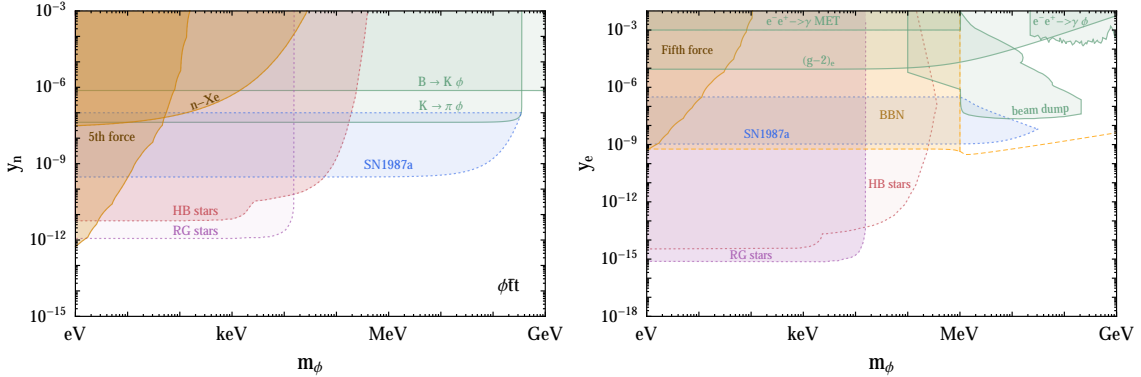


Figure 3. Constraints on (*left*) mediator-nucleon coupling $\mathcal{L} = y_n \phi \bar{n} n$ (mediated by a top quark) and (*right*) mediator-electron coupling $\mathcal{L} = y_e \bar{e} e$, as a function of the mediator mass. Figures taken from Ref. [24].

- *Invisible decays.* In this case the mediator either decays dominantly to DM, or is stable on detector timescales. If the mediator couples to hadrons and is lighter than Λ_{QCD} , it can be constrained through the invisible processes $B \rightarrow K\phi$ and $K \rightarrow \pi\phi$, where ϕ is a scalar or vector mediator [24]. The effective coupling to nucleons constrained in this way is $y_n \lesssim 10^{-5} - 10^{-7}$, depending on the flavor structure of the ϕ -quark coupling. If the mediator couples to electrons, it can be constrained by $e^+e^- \rightarrow \gamma\phi$, *i.e.* a mono-photon search in BaBar. The electron $(g-2)$ measurement also provides a powerful bound. See Refs. [24, 59, 60] for a summary of collider bounds.
- *Visible decays.* Here, the constraints are strongest when the mediator is produced, and decays directly to charged leptons $\ell^+\ell^-$ [61, 62]. These constraints are typically labeled as “beam dump” constraints.

While we have not exhaustively summarized the collider probes on light hidden sectors, these summarize the general types of constraints on mediators. We show two summary plots in Fig. 3, for nucleon and lepton couplings, that demonstrate the collider, stellar, and fifth force bounds on the nucleon or electron-scalar couplings.

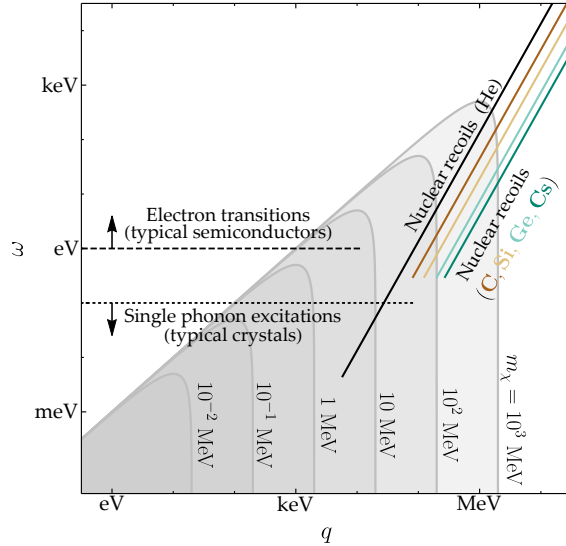


Figure 4. The kinematic parameter space of light DM, in terms of the energy deposition ω and momentum transfer q in a direct detection experiment. The shaded parabolas correspond to the range of energy and momentum a DM particle of a given mass can deposit (Eq. 34). The nuclear recoil curves correspond to the energy deposit on a nucleus, Eq. 36. The horizontal lines at an eV and 100 meV correspond to the energy gaps (as $q \rightarrow 0$) of electronic excitations (in semiconductors) and optical phonons (in crystals). Figure reproduced from Ref. [63].

V. DIRECT DETECTION OF LIGHT PARTICLE DARK MATTER

The direct detection of light DM depends on considerations of both kinematics and interactions. That is, one needs to find a target material with a strong response (or “dynamic structure factor”) for energy and momentum deposition in the DM kinematic regime, for the relevant type of interaction. We briefly summarize both before describing the particular mechanisms for detection of light DM.

In direct detection, DM must be able to cause a transition from an initial to final state $|i\rangle \rightarrow |f\rangle$ of the target system, with the DM typically depositing some momentum $\mathbf{q} = \mathbf{p} - \mathbf{p}'$, where $\mathbf{p} = m_\chi \mathbf{v}$, \mathbf{p}' are the initial and final DM momentum, which corresponds to some energy ω deposited by the DM on the target:

$$\omega = \frac{1}{2}m_\chi v^2 - \frac{(m_\chi \mathbf{v} - \mathbf{q})^2}{2m_\chi} = \mathbf{q} \cdot \mathbf{v} - \frac{q^2}{2m_\chi}. \quad (33)$$

Note that this expression assumes that the DM has no internal excitations (such as energy

levels) that could cause the transition to be inelastic on the DM side. The energy deposited is bounded by a parabola,

$$\omega \leq qv_{\max} - q^2/2m_\chi, \quad (34)$$

as first illustrated in Ref. [63] and reproduced in Fig. 4. This figure shows the basic kinematic requirements of a material in order to allow for a detection event: the target material must have a state whose transition energy and momentum lie below (and within) the DM kinematic parabola. In addition, the closer a mode in the material is to the upper part of the parabola, the more energy can be read out, allowing in many cases for a more viable path toward detection. DM can never transfer more momentum than

$$q_{BW} = 2m_\chi v_{\max}, \quad (35)$$

the “brick wall” limit where little energy is deposited corresponding to the right edge of the DM kinematic parabola. Take for example the case of nuclear recoils, where the energy deposit is

$$\omega = \frac{q^2}{2m_N}, \quad (36)$$

where m_N is the target nucleus mass, also shown on the figure. At the point where the nuclear recoil kinematic curve intersects the DM parabola, only a small fraction of the DM kinetic energy is deposited onto the nucleus,

$$\omega = \frac{2m_\chi^2 v^2}{m_N} \ll \frac{m_\chi v^2}{2}, \quad (37)$$

when the DM is lighter than typical SM nuclei mass. One immediately sees that sub-GeV DM is kinematically poorly matched to SM nuclei, and one should search for other targets for DM interactions. We now summarize the types of excitations that are relevant in each mass regime.

A. Targets and Excitations for Dark Matter Interactions

- For DM with mass $\gtrsim 30$ MeV, **nuclear recoils** are a relevant target, though they extract only a small fraction of the DM kinetic energy. Since the DM energy deposition

is given in Eq. 36, in order to extract the maximum energy deposition ω the lightest target is preferable. In particular, superfluid helium has been identified as a promising target for the TESSERACT DM experiment. The lower end of the DM mass range $m_\chi \gtrsim 30$ MeV corresponds to DM energy deposit on nuclei via Eq. 36 larger than $\omega \gtrsim 500$ meV corresponding to the typical energy of collective excitations, where the nucleus can no longer be treated as free (see discussion in Ref. [63]). For smaller energy depositions, the relevant excitations are phonons.

- For DM with mass $m_\chi \gtrsim 1$ MeV, having kinetic energy $\omega \gtrsim 1$ eV, **electrons** in targets such as semiconductors (having a typical band-gap of 1 eV) and ionization in noble liquids such as Xenon (with ionization threshold of ~ 10 eV) are good targets, and have been explored extensively [64–66]. Ripping an electron out of a 2-d material such as graphene, with a work function also in the 1 eV energy range [67] and chemical bonds [68] having energy in the 10’s of eV range have also been proposed.
- At slightly lower energy depositions, in the 100 meV range, **collective excitations** such as optical phonons (gapped excitations having energy ω_{ph}) become available and have been proposed as a viable pathway [50, 69], having greatest sensitivity via scattering for DM in the $m_\chi \gtrsim$ keV-MeV mass range. Collective excitations are highly sensitive to heavier DM as long as the momentum transfer is smaller than that required to kick the ion out of the lattice potential $q \lesssim \sqrt{2m_N\omega_{\text{ph}}} \sim 10 - 100$ keV. This momentum corresponds to that carried by MeV mass DM in the Milky Way, though for heavier DM only a small fraction of its total momentum may be transferred, especially if the mediator is light, having a $1/q^4$ enhancement in the cross-section as in Eq. 4 with $m_M \rightarrow 0$. See Ref. [69] for a detailed analysis. The SPICE (sub-eV Polar Interactions Cryogenic Experiment) experiment has research underway to detect single phonons in crystals [70]. In addition to phonons, magnons are a different type of collective excitation in materials that can detect spin-dependent DM interactions [71].
- Other gapped excitations, such as vibrational degrees of freedom in organics [72], and electronic excitations with small gaps, such as occurs in superconductors [49, 73], Dirac materials [67, 74], heavy fermion materials [75], and doped semiconductors [76] are also viable targets for $m_\chi \gtrsim$ keV DM.

So far, we have explored the importance of kinematic matching between DM and target. We now examine the strength of the target response to a given energy ω and momentum \mathbf{q} deposition. This requires computing the quantum mechanical matrix element entering into Fermi's Golden Rule for interaction rates. The matrix element in turn depends on the interaction type, such as spin-independent (SI), spin-dependent (SD), or a more generic interaction such as an electric or magnetic dipole or anapole. In the next sub-sections, we lay out the general quantum mechanical framework for computing the rate, and then apply it to SI scattering. In Sec. VI A, we will consider more general interactions in an Effective Field Theory (EFT) framework.

B. Quantum Mechanics of Dark Matter Scattering

The interaction type enters directly into the calculation of the matrix element for the DM to induce a transition from an initial to a final state in a target material. The DM deposits some energy and momentum, (ω, \mathbf{q}) within the kinematically allowed DM parabola shown in Fig. 4, and the over-arching goal is to find a material with a strong quantum mechanical response, encapsulated in a Dynamic Structure Factor. See Refs. [63, 77] for a more complete discussion of the physics reviewed here.

Quantum mechanics enters in determining the transition rate from initial to final state of the target material $|i\rangle \rightarrow |f\rangle$, via a simple application of Fermi's Golden Rule:

$$\Gamma(\mathbf{v}) = V \int \frac{d^3q}{(2\pi)^3} \sum_f |\langle \mathbf{p}', f | H_{\text{int}} | \mathbf{p}, i \rangle|^2 2\pi \delta(E_f - E_i - \omega), \quad (38)$$

where H_{int} is the interaction Hamiltonian, and we will assume throughout that the DM state factorizes from the target state (since they are unentangled), $|\mathbf{p}, i\rangle = |\mathbf{p}\rangle \otimes |i\rangle$, *etc.*, and V is the volume of the target. The interaction rate in Eq. 45 depends on the DM velocity \mathbf{v} , whose typical value in the Milky Way galaxy is $v \sim 10^{-3}$. The detectable interaction rate, per unit target mass, is extracted by integrating over the DM velocity phase space:

$$R = \frac{1}{\rho_T} \frac{\rho_\chi}{m_\chi} \int d^3v f_\chi(\mathbf{v}) \Gamma(\mathbf{v}), \quad (39)$$

with $\rho_{\chi,T}$ being the DM and target densities, and f_χ typically taken to be a Maxwell-Boltzmann distribution, truncated at the escape velocity $v_{\text{esc}} \sim 600$ km/s of the DM from the galaxy. Note that while $\Gamma(\mathbf{v})$ is a rate, R is a rate per unit mass.

1. *Example: Spin-Independent Scattering*

To illustrate the principles discussed above, we first consider DM scattering via a spin-independent interaction. The DM creates a potential

$$\langle \mathbf{p}' | H_{\text{int}} | \mathbf{p} \rangle = V(\mathbf{q}) \quad (40)$$

to which the target responds. It is convenient to factorize this potential into a material response \mathcal{F}_T (which is agnostic about the DM) and a DM matrix element \mathcal{M} (which is agnostic about the target):

$$V(\mathbf{q}) = \mathcal{M}(q)\mathcal{F}_T(\mathbf{q}). \quad (41)$$

For spin-independent scattering, the DM-induced potential $\mathcal{M}(q)$ is characterized by a fiducial cross-section and a mediator form factor

$$\mathcal{M}(q) = \mathcal{M}(q_0)\mathcal{F}_{\text{med}}(q), \quad (42)$$

where $\mathcal{F}_{\text{med}}(q)$ is either 1 (for a heavy mediator) or $(q_0/q)^2$ (for a light mediator with momentum dependence typical of Rutherford scattering). $\mathcal{M}(q_0)$ is related to a reference cross-section convenient for parameterizing the overall strength of the interaction via

$$\bar{\sigma}_T \equiv \frac{\mu_{\chi T}^2}{\pi} |\mathcal{M}_{\chi T}(q_0)|_{q_0=m_{\chi}v_0}^2, \quad (43)$$

where $\mu_{\chi T}$, with $T = n, e$ denotes the DM-target (nucleon or electron) reduced mass. The target response $\mathcal{F}_T(q)$, for spin-independent interactions, is traditionally absorbed into what is known as the *dynamic structure factor*, which characterizes the response of the material:

$$S(\mathbf{q}, \omega) \equiv \frac{1}{V} \sum_f |\langle f | \mathcal{F}_T(\mathbf{q}) | i \rangle|^2 2\pi \delta(E_f - E_i - \omega), \quad (44)$$

where E_f, E_i are the final and initial energies of the target. The formalism where the DM scattering rate is proportional to the dynamic structure factor is valid as long as the scattering is spin-independent. Below we will generalize the calculation to a generic type of potential, including spins; however for intuition, and to match to the standard Condensed Matter (CM) understanding, we start with the spin-independent case. The DM-target scattering rate can thus be written in a unified way in terms of the dynamic structure factor:

$$\Gamma(\mathbf{v}) = \frac{\pi \bar{\sigma}}{\mu^2} \int \frac{d^3 q}{(2\pi)^3} \mathcal{F}_{\text{med}}^2(q) S(\mathbf{q}, \omega). \quad (45)$$

The three basic types of spin-independent interactions we will consider in the next subsection—nuclear recoil, electron excitation, and phonon excitation—can be expressed in terms of the dynamic structure factor. We will see that we can reproduce the results in the literature utilizing this simple unifying language. The dynamic structure factor is a material-specific response that depends kinematically only on the input (\mathbf{q}, ω) provided by the DM interaction. The dynamic structure factor can be generalized from spin-independent interactions, within an EFT framework, but utilizing the same basic tools introduced here. We take on that task in the next section, but first summarize the broad types of interactions utilized for light DM detection: nuclear recoil, electronic excitations, and single phonon excitation, in the language of the dynamic structure factor.

Nuclear recoils. In the case of nuclear recoils, for each species of nucleus, the dynamic structure factor is

$$S(\mathbf{q}, \omega) = 2\pi \frac{\rho_T}{m_N} \frac{f_N^2}{f_n^2} F_N^2(q) \delta\left(\frac{q^2}{2m_N} - \omega\right), \quad (46)$$

where m_N is the target nucleus mass, $F_N(q)$ is the nuclear form factor (often taken to be the Helm form factor), f_N is the coupling to the nucleus, and f_n is the coupling to a nucleon which we divide through by convention to cancel the same coupling in the cross-section Eq. 43. Note that a single nucleus response is appropriate as long as the nucleus can be treated as free. This occurs when the energy deposition is greater than a typical phonon energy, $\omega \gg \omega_{\text{ph}} \simeq 10 - 500$ meV, or equivalently, $q \gg \sqrt{m_N \omega_{\text{ph}}}$.

Electronic excitations. At the next level of complexity and at lower energy depositions and momentum transfer, DM interactions can induce electronic transitions. In this case, the dynamic structure factor depends on the electron wavefunctions in the initial and final state:

$$S(\mathbf{q}, \omega) = \frac{2\pi}{V} \left(\frac{f_e}{f_e^0}\right)^2 \sum_{i,f} \delta(E_f - E_i - \omega) \left| \int \frac{d^3 k'}{(2\pi)^3} \frac{d^3 k}{(2\pi)^3} (2\pi)^3 \delta^3(\mathbf{k}' - \mathbf{k} - \mathbf{q}) \psi_f^*(\mathbf{k}') \psi_i(\mathbf{k}) \right|^2,$$

where the sum over i, f is over all the initial and final electronic states whose energy difference is $\omega = E_f - E_i$. In a semiconductor, the relevant states are core, valence, conduction and free electrons, where the wavefunctions are written in terms of Bloch waves labeled by a band index I and wavenumber \mathbf{k} :

$$\psi_{I,\mathbf{k}}(\mathbf{x}) = \frac{1}{\sqrt{V}} \sum_{\mathbf{G}} u_I(\mathbf{k} + \mathbf{G}) e^{i(\mathbf{k} + \mathbf{G}) \cdot \mathbf{x}}. \quad (47)$$

This immediately leads to a dynamic structure factor

$$S(\mathbf{q}, \omega) = \frac{2}{V} \sum_{i,f} \int_{\text{1BZ}} \frac{d^3 k_1}{(2\pi)^3} \frac{d^3 k_2}{(2\pi)^3} 2\pi \delta(E_{f,\mathbf{k}_2} - E_{i,\mathbf{k}_1} - \omega) \times \left| \sum_{\mathbf{G}_1, \mathbf{G}_2} (2\pi)^3 \delta^3(\mathbf{k}_2 + \mathbf{G}_2 - \mathbf{k}_1 - \mathbf{G}_1 - \mathbf{q}) u_f^*(\mathbf{k}_2 + \mathbf{G}_2) u_i(\mathbf{k}_1 + \mathbf{G}_1) \right|^2, \quad (48)$$

where the prefactor of 2 comes from summing over degenerate spins. Now we can define a crystal form factor with an Umklapp \mathbf{G} , which allows us to take into account in momentum space the periodicity of the crystal lattice,

$$f_{[i,\mathbf{k}_1,f,\mathbf{k}_2,\mathbf{G}]} \equiv \sum_{\mathbf{G}_1, \mathbf{G}_2} u_f^*(\mathbf{k}_2 + \mathbf{G}_2) u_i(\mathbf{k}_1 + \mathbf{G}_1) \delta_{\mathbf{G}_2 - \mathbf{G}_1, \mathbf{G}}, \quad (49)$$

so that we can rewrite the dynamic structure factor as

$$S(\mathbf{q}, \omega) = \frac{2}{V} \sum_{i,f} \int_{\text{1BZ}} \frac{d^3 k_1}{(2\pi)^3} \frac{d^3 k_2}{(2\pi)^3} 2\pi \delta(E_{f,\mathbf{k}_2} - E_{i,\mathbf{k}_1} - \omega) \times \sum_{\mathbf{G}} (2\pi)^3 \delta^3(\mathbf{k}_2 - \mathbf{k}_1 - \mathbf{G} - \mathbf{q}) |f_{[i,\mathbf{k}_1,f,\mathbf{k}_2,\mathbf{G}]}|^2. \quad (50)$$

This formula can also be applied to the case of superconductors, where the calculation is relatively simple because, for energy depositions well above the Cooper pair binding energy, the electrons behave as free particles in a Fermi-degenerate sea. In that case, $\mathbf{G} = 0$ and the crystal form factor is simply replaced by the Fermi-Dirac distributions

$$|f_{[i,\mathbf{k}_1,f,\mathbf{k}_2,\mathbf{G}]}|^2 = f(\omega_{k_1})(1 - f(\omega_{k_2})), \quad (51)$$

where $f(E_i) = [1 + \exp(\frac{E_i - \mu_i}{T})]^{-1}$ is the Fermi-Dirac distribution of electrons at temperature T . In the limit $T \rightarrow 0$, the dynamic structure factor reduces to [49]

$$S(\omega, \mathbf{q}) \simeq \frac{m_e^2 \omega}{\pi q} \Theta(qv_F - \omega), \quad (52)$$

where $v_F \simeq 10^{-2}$ is the Fermi velocity of electrons in a superconductor.

The technical obstruction to computing DM interaction rates in materials like semiconductors is the electronic wavefunctions. In some cases, especially where the electrons are more tightly bound [78], analytic atomic wavefunctions can provide an approximation that gives correct order-of-magnitude estimates for DM interaction rates [79, 80]. However, especially

for conduction electrons, these approximations are not very good, and there now exist multiple codes to compute spin-independent scattering rates of light DM electrons utilizing wavefunctions computed via Density Functional Theory (DFT). This includes the QEDark [66] and QCDark [81], EXCEED-DM [78, 82] and DarkELF [83] packages. EXCEED-DM extended QEDark by including the all-electron reconstructed wavefunctions and additional electronic states outside of valence and conduction bands. DarkELF makes use of the DFT-computed dielectric function $\epsilon(\omega, \mathbf{q})$, with the observation that the dynamic structure function, *for dark photon-like scattering on electrons*, can be written in the low-temperature limit as [75, 84]

$$S(\omega, \mathbf{q}) = \frac{q^2}{2\pi\alpha_{em}} \text{Im} \left[\frac{-1}{\epsilon_L(\omega, \mathbf{q})} \right]. \quad (53)$$

This can be a convenient expression for spin-independent scattering, if the dielectric function is available for all (ω, \mathbf{q}) of interest.

We summarize in Table I the types of targets, and their gaps, proposed for DM interacting with the electron. There are already many experiments in process that realize these ideas:

- Ionization in atoms and excitation across the band gap in semiconductors were the first proposal to detect MeV-GeV DM, and is currently being implemented in semiconductor targets of SuperCDMS, SENSEI, DAMIC and EDELWEISS. The Xenon (PandaX, Xenon1T, LUX) and liquid argon (DarkSide) experiments have also done searches for ionization of electrons.
- Cooper-pair breaking in superconductors has been implemented to search for keV-GeV light DM with superconducting nanowires (SNSPDs) [85].

We refer the reader to Ref. [86] (especially Figure 1) for a currently complete discussion of the ongoing experimental efforts, which we do not attempt to cite in detail here.

Single Phonon excitations. When the energy deposition drops below $\omega \sim 100 \text{ meV} \sim q^2/2m_N$, with $q \sim 10 - 100 \text{ keV}$, the nucleus can no longer be treated as free and the relevant degrees-of-freedom are no longer single ions. Phonons are collective oscillations of atoms in fluids (such as superfluid helium) or crystals (including metals like superconductors). For a crystal with a lattice structure having n ions in a unit cell, there are $3n$ such modes. Three of those modes are gapless acoustic phonons; theoretically these modes are Goldstone Bosons

Target	Reaction Process	typical gap	Elastic or Inelastic?	DM Mass Range
Atom	Ionization	10 eV	Inelastic	$\gtrsim 10$ MeV-GeV
Semiconductor	Excitation across band gap	~ 1 eV	Inelastic	MeV-GeV
Superconductor	Cooper pair breaking	~ 1 meV	approx. Elastic	$\gtrsim 1$ keV-GeV
Graphene	Electron ejection	~ 1 eV	Inelastic	$\gtrsim 1$ MeV-GeV
Dirac Material	Excitation across band gap	$\sim 0 - 1$ meV	Inelastic	keV-GeV
Heavy Fermion Material	Excitation across band gap	~ 10 meV	Inelastic	10 keV-GeV

Table I. Summary of the target materials that have been proposed for DM detection through electron excitation. The superconductor DM detection process is elastic for energy depositions well above the Cooper pair binding energy.

of broken translation symmetry, and physically correspond to the ions oscillating together in-phase in each of the three spatial directions. The dispersion of these modes is given by

$$\omega = c_s q, \quad (54)$$

where c_s is the speed of sound in the medium. Any remaining modes are gapped, meaning that at zero momentum transfer they have a non-zero excitation energy. All of these modes physically correspond to out-of-phase oscillations of the ions, which can set up an oscillating dipole in the unit cell. The gapped phonons are called optical phonons, because at least *some* of these modes are optically active. A typical band structure is shown in Fig. 5.

Similar to the previous cases, the spin-independent scattering rate can be expressed in terms of a dynamic structure factor

$$S(\mathbf{q}, \omega) = \sum_{\nu} \frac{|F_{\nu}(\mathbf{q})|^2}{2\omega_{\nu, \mathbf{q}}} \delta(\omega_{\nu, \mathbf{q}} - \omega), \quad (55)$$

where $\omega_{\nu, \mathbf{q}}$, $\epsilon_{\nu, \mathbf{q}, j}$ are the eigenvalues and eigenvectors of phonon branch ν (with the polarization vector indicating the direction in which ion j is oscillating, normalized such that $\sum_j |\epsilon_{\nu, \mathbf{q}, j}|^2 = 1$) of the coupled ionic oscillators, and $F_{\nu}(\mathbf{q})$ is a phonon form factor

$$|F_{\nu}(\mathbf{q})|^2 = \left| \sum_j \frac{e^{-W_j(\mathbf{q})}}{\sqrt{m_j}} \mathbf{q} \cdot \epsilon_{\nu, \mathbf{q}, j} e^{-i\mathbf{q} \cdot \mathbf{x}_j^0} \right|^2. \quad (56)$$

Here the sum runs over the ions at equilibrium position \mathbf{x}_j^0 in the unit cell and W_j is the so-called Debye-Waller factor that acts as a form factor shutting off the phonon response

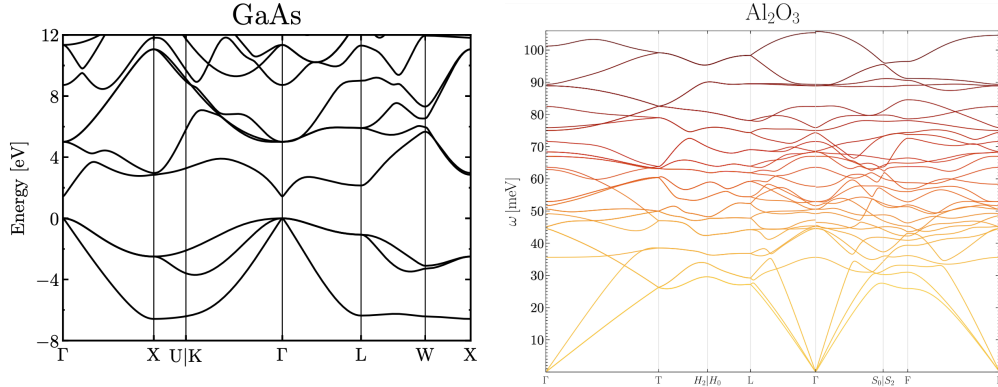


Figure 5. Band structure of two materials. *Left*: Electronic excitations in a semiconductor, GaAs. The Fermi energy defines the 0 point on the y -axis, with the valence and conduction bands below and above the Fermi energy. On the x -axis, a slice is taken through the Brioullin zone to show a typical band structure. The Γ point is defined by where the bands come closest to crossing the Fermi surface. *Right*: Phonon excitations in a polar material, sapphire. Here the excitation energies ω are above the zero energy state with no phonons. The Γ point is again defined by the point in momentum space where the gapless acoustic modes have zero energy, such that their dispersion is given by Eq. 54. The gapped phonons are called optical, even though not all of these modes are optically active. Figures reproduced from Ref. [69].

when the momentum transfer becomes larger than the inverse unit cell size $q \gtrsim a^{-1}$ (see Refs. [50, 63, 87] for a derivation and discussion). The eigenvalues and eigenvectors are typically obtained from a program like `phonopy` that computes the lattice force matrix on all n ions in the unit cell and diagonalizes it.

Operationally, the phonon form factor behaves similarly to the Helm form factor, in that it becomes highly suppressed when the effective description of collectively oscillating ions (or in the case of the Helm, collective nucleons in a nucleus) breaks down due to resolving the internal structure of the unit cell. In particular, one can see explicitly that when the momentum transfer becomes large in comparison to the typical momentum in a mode, $q^2 \gg 2\omega_{\nu,q}m_j$, the Debye-Waller factor becomes large:

$$W_j(\mathbf{q}) = \frac{1}{4m_j} \sum_{\nu} \int_{\text{1BZ}} \frac{d^3k}{(2\pi)^3} \frac{|\mathbf{q} \cdot \epsilon_{\nu,\mathbf{k}j}|^2}{\omega_{\nu,\mathbf{k}}}, \quad (57)$$

and hence the dynamic structure factor via the phonon form factor in Eq. 56 becomes small.

(Here the momentum has been integrated over the first Brillouin Zone (BZ), see Ref. [63] for more detail.) At a general momentum transfer, the phase factors, and in particular cancellations between the phase factors, can become important for accurately describing the DM interaction rate with phonons. However, at low momentum transfer, where the Debye-Waller factor is small, the form factor takes a simple form. For example, in a simple crystal like GaAs where there are only two ions in the unit cell, we have

$$|F_\nu(\mathbf{q})|^2 \approx \frac{q^2}{2m_n} \left| \sqrt{A_{\text{Ga}}} e^{i\mathbf{x}_{\text{Ga}} \cdot \mathbf{q}} \pm \sqrt{A_{\text{As}}} e^{i\mathbf{x}_{\text{As}} \cdot \mathbf{q}} \right|^2, \quad (58)$$

where $\mathbf{x}_{\text{Ga,As}}$, $A_{\text{Ga,As}}$ denote the positions and mass numbers of the gallium and arsenide ions in the unit cell, respectively [50]. In general, however, one uses codes employing DFT to compute the phonon eigenvectors and eigenfrequencies [63, 87]. This general program was outlined first in Ref. [63], and a code implementing this program in a variety of materials is publicly available as the PhonoDark code [77, 88]. This code implements not only spin-independent interactions, but also follows a general framework for calculating the DM single-phonon excitation rate via any Lorentz-Invariant effective interaction. We will describe this framework in the next section.

There are now experimental efforts underway to detect single collective excitations:

- The TESSERACT collaboration, consisting of the helium experiment HeRALD and the polar material experiment SPICE, is actively working to reach single optical phonon sensitivity with the transition edge sensors (TES) employed in the detector.
- At present, the single magnon proposal of Refs. [71, 89] is not experimentally implemented, though a related concept (through many magnons) forms the basis of the QUAX experiment [90].

A summary of the collective modes, possible targets, gap of the collective mode and coupling (nucleon or electron) is given in Table II. We again refer the reader to Ref. [86] for a currently complete discussion of ongoing experimental efforts.

An additional comment is in order: at typical energies above the higher optical mode (typically $\omega \sim 100$ meV) but below where the nucleus becomes definitely free $\omega \sim 1$ eV, multi-phonon emission becomes important. The calculation of multi-phonon processes can rapidly become numerically intensive, due to the large multi-phonon phase space, and the

Collective Mode	Target	Proposed Materials	Gap?	Coupling
Acoustic Ph.	All materials	He, Si, Ge, GaAs, Al ₂ O ₃ , diamond	no	$p/n/e^-$
Optical Ph.	Polar, semicond.	GaAs, Al ₂ O ₃	$\sim 10 - 100$ meV	$p/n/e^-$
Magnon	(anti-)ferromagnet	YIG	$\sim 0 - 10$ meV	e^-

Table II. Summary of the target materials that have been proposed for DM detection through collective excitations. The superconductor DM detection process is elastic for energy depositions well above the Cooper pair binding energy.

presence of both harmonic and anharmonic multi-phonon modes. Two-phonon production as a means to detect light DM was proposed in Ref. [91, 92], and calculated in an EFT in Refs. [93, 94]. The harmonic contributions can be computed using analytic methods, and the results applied to interpolate between the single phonon regime valid at low energies and the nuclear recoil regime [95], and the effect of anharmonicities estimated [96]. Note that even single phonon production, initially, will lead to the cascade of multi-phonons [97] as the initial phonon decays through the anharmonic coupling, in a process rather analogous to showering.

C. In-medium Effects

Small gap electronic materials have a large in-medium response that affects reach to DM scattering and absorption through screening effects. For isotropic, non-magnetic materials interacting through a dark photon, the effect of the in-medium response can be parameterized in terms of a reduced effective kinetic mixing parameter ϵ_{eff} [24, 49]:

$$\epsilon_{\text{eff}} = \epsilon \frac{q^2}{q^2 - \Pi_{T,L}}, \quad (59)$$

where $\Pi_{T,L}$ is the in-medium polarization tensor of an isotropic, non-magnetic material, related to the complex index of refraction \tilde{n} by $q^2(1 - \tilde{n}^2) = \Pi_L$, $\omega^2(1 - \tilde{n}^2) = \Pi_T$. The case of an anisotropic material is significantly more involved [98], where the in-medium effects must be written in terms of a tensor, whose eigenvalues are given by

$$\pi_i = \omega^2(1 - \epsilon_{ii}), \quad (60)$$

with the effective mixing parameter

$$\epsilon_{\text{eff},i}^2 = \frac{\epsilon^2 m_{A'}^4}{[m_{A'}^2 - \text{Re}\pi_i(q)]^2 + [\text{Im}\pi_i(q)]^2}. \quad (61)$$

We discuss below how these effective couplings enter into the absorption rate.

VI. GENERALIZED DARK MATTER INTERACTIONS

We have summarized the relevant ingredients for DM to induce a response in a target material. We now generalize the framework to an EFT of DM scattering in the next Subsection, followed by general considerations on DM absorption in target materials.

A. Effective Field Theory of Dark Matter Scattering with Collective Excitations

As suggested in Eq. 44, one needs to be able to compute the transition matrix element $\langle f | \mathcal{F}_T(\mathbf{q}) | i \rangle$ for any interaction type in order to be able to compute the DM scattering rate for any interaction type. This in turn implies that we must be able to compute the potential, the generalization of Eq. 41, that the DM induces in the target material. DM is a non-relativistic (NR) state, and therefore one needs to follow the rules of NREFT. The discussion here largely follows Ref. [77].

For scattering, the EFT calculation follows a simple plan:

1. Match relativistic operators onto non-relativistic operators. There is a long history in the nuclear physics literature of identifying the relevant NR operators. They are

$$\mathbf{q} \equiv \mathbf{k}' - \mathbf{k}, \quad \mathbf{K} \equiv \mathbf{k}' + \mathbf{k}, \quad \mathbf{S}_\psi, \quad \mathbf{v}_\chi \equiv \frac{\mathbf{P}}{2m_\chi}, \quad \mathbf{v}_\psi \equiv \frac{\mathbf{K}}{2m_\psi}. \quad (62)$$

Here m_ψ is the target fermion mass and \mathbf{S}_ψ the spin. Note that in the nuclear recoil case, Galilean invariance is preserved, and the NREFT depends only on $\mathbf{v}^\perp \equiv \mathbf{v}_\chi - \mathbf{v}_\psi$. In the present case, in-medium effects may be important, and Galilean invariance is broken such that we need to keep both.

2. Eq. 62 identifies charge, spin and velocity operators as being relevant to determining the potential created by the DM-target interaction. In particular, the transition matrix element induced by a potential, generalized from Eq. 41 to include velocity and

momentum dependence, is

$$\langle \nu, \mathbf{k} | \tilde{V}(\mathbf{q}, \mathbf{v}) | 0 \rangle = \sum_{\ell, j} \langle \nu, \mathbf{k} | e^{-i\mathbf{q} \cdot \mathbf{x}_{\ell j}} \tilde{V}_{\ell j}(\mathbf{q}, \mathbf{v}) | 0 \rangle \quad (63)$$

where ℓ labels the unit cell, j the ion within the unit cell, and the subscripts on the potential denote the contribution from each lattice site:

$$V(\mathbf{x}, \mathbf{v}) = \sum_{\ell j} V_{\ell j}(\mathbf{x} - \mathbf{x}_{\ell j}, \mathbf{v}), \quad (64)$$

with

$$\tilde{V}(\mathbf{q}, \mathbf{v}) = \int d^3x e^{-i\mathbf{q} \cdot \mathbf{x}} V(\mathbf{x}, \mathbf{v}). \quad (65)$$

The transition is between the ground state of the material $|0\rangle$ and a state with a single collective excitation, labeled by $|\nu, \mathbf{k}\rangle$. Below, we will give two examples of how to compute the DM-induced lattice potential. Because in what follows we exclusively utilize the potential in momentum space, we will drop the tilde on $\tilde{V}(\mathbf{q}, \mathbf{v})$ for readability.

3. Finally we quantize the lattice potential to compute the matrix element. There are two quanta that are excitations of the lattice potential that we consider.

- *Phonons.* Phonons are quanta of lattice displacement $\mathbf{u}_{\ell j}$ from the equilibrium ion position at site j in the ℓ th unit cell $\mathbf{x}_{\ell j}^0$:

$$\mathbf{u}_{\ell j} = \mathbf{x}_{\ell j} - \mathbf{x}_{\ell j}^0 = \sum_{\nu=1}^{3n} \sum_{\mathbf{k}} \frac{1}{\sqrt{2Nm_j\omega_{\nu, \mathbf{k}}}} \left(\hat{a}_{\nu, \mathbf{k}} \epsilon_{\nu, \mathbf{k}, j} e^{i\mathbf{k} \cdot \mathbf{x}_{\ell j}^0} + \hat{a}_{\nu, \mathbf{k}}^\dagger \epsilon_{\nu, \mathbf{k}, j}^* e^{-i\mathbf{k} \cdot \mathbf{x}_{\ell j}^0} \right), \quad (66)$$

where N is the number of cells in the lattice, m_j is the mass of the ion at the j th site, and we have added subscripts on the energy deposition $\omega_{\nu, \mathbf{k}}$ (where the momentum \mathbf{k} is in the first Brillouin zone) to emphasize that the energy deposition must correspond to the energy of one of the eigenfrequencies of the collective excitations. Since the matrix element we seek to compute involves the potential Eq. (65) with a factor of $e^{i\mathbf{q} \cdot \mathbf{x}_{\ell j}}$, the matrix element must be evaluated via Campbell-Baker-Hausdorff (CBH) to give

$$\langle \nu, \mathbf{k} | e^{-i\mathbf{q} \cdot \mathbf{x}_{\ell j}} V_{\ell j}(\mathbf{q}, \mathbf{v}) | 0 \rangle = \frac{1}{\sqrt{V}} \sum_{\nu, \mathbf{k}, j} \left[\sum_{\ell} V_{\ell j}(\mathbf{q}, \mathbf{v}) e^{i(\mathbf{q}-\mathbf{k}) \cdot \mathbf{x}_{\ell j}^0} \right] \frac{e^{-W_j(\mathbf{q})} (\mathbf{q} \cdot \epsilon_{\nu, \mathbf{k}, j}^*)}{\sqrt{2m_j\omega_{\nu, \mathbf{k}}}},$$

where Debye-Waller factor W_j is derived here from the application of CBH (the derivation can be found in Ref. [63]). The task is then to evaluate the lattice potential, $V_{\ell j}(\mathbf{q}, \mathbf{v})$. This depends on the nature of the interaction. Utilizing an example from Ref. [77], involving four different types of responses, a lattice potential may take the form:

$$V_{\ell j}(\mathbf{q}, \mathbf{v}) \supset \sum_{\alpha} \left[c_1 \langle e^{i\mathbf{q}\cdot\mathbf{x}_{\alpha}} \rangle_{\ell j} + c_4 \mathbf{S}_{\chi} \cdot \langle e^{i\mathbf{q}\cdot\mathbf{x}_{\alpha}} \mathbf{S}_{\alpha} \rangle_{\ell j} \right. \\ \left. + c_{8b} \mathbf{S}_{\chi} \cdot \langle e^{i\mathbf{q}\cdot\mathbf{x}_{\alpha}} \mathbf{v}_{\alpha} \rangle_{\ell j} + c_{3b} \frac{i\mathbf{q}}{m_{\psi}} \cdot \langle e^{i\mathbf{q}\cdot\mathbf{x}_{\alpha}} \mathbf{v}_{\alpha} \times \mathbf{S}_{\alpha} \rangle_{\ell j} \right]. \quad (67)$$

A spin-independent interaction requires one to evaluate the matrix element

$$\sum_{\alpha} \langle e^{i\mathbf{q}\cdot\mathbf{x}_{\alpha}} \rangle_{\ell j} \simeq \langle N_{\psi} \rangle_{\ell j} \quad (68)$$

where α runs over fermions of type $\psi = p, n, e$. Likewise, a spin-dependent interaction requires one to evaluate

$$\sum_{\alpha} \langle e^{i\mathbf{q}\cdot\mathbf{x}_{\alpha}} \mathbf{S}_{\psi, \alpha} \rangle_{\ell j} \simeq \langle \mathbf{S}_{\psi} \rangle_{\ell j}. \quad (69)$$

Coupling to electric and magnetic dipoles, as well as the anapole operator, involve the velocity $\mathbf{v}_{\psi, \alpha} = -\frac{i}{2m_{\psi}} \overleftrightarrow{\nabla}$ and one must evaluate the expectation value

$$\sum_{\alpha} \langle e^{i\mathbf{q}\cdot\mathbf{x}_{\alpha}} \mathbf{v}_{\psi, \alpha} \rangle_{\ell j} \simeq i \langle (\mathbf{q} \cdot \mathbf{x}_{\alpha}) \mathbf{v}_{\psi, \alpha} \rangle_{\ell j}, \quad (70)$$

which becomes

$$\langle x_{\alpha}^i v_{\psi, \alpha}^k \rangle_{\ell j} = -\frac{i}{2m_{\psi}} \langle x^i \nabla_{\alpha}^k - x^k \nabla_{\alpha}^i \rangle_{\ell j} = \frac{1}{2m_{\psi}} \epsilon_{ik k'} \langle L_{\alpha}^{k'} \rangle_{\ell j}, \quad (71)$$

where L is an angular momentum operator. Overall, one finds, in the long-wavelength limit, that there are four types of responses:

$$N, \quad S, \quad L, \quad L \otimes S, \quad (72)$$

where we have not written out the decomposition of the last operator because it does not commonly appear in Lorentz-invariant UV-completions.

- *Magnons.* Magnons are quanta of spin precession. Here, the relevant matrix element is

$$\langle \nu, \mathbf{k} | V(\mathbf{q}, \mathbf{v}) | 0 \rangle = \sum_{\ell, j} e^{i\mathbf{q}\cdot\mathbf{x}_{\ell j}} \mathbf{f}_j(\mathbf{q}, \mathbf{v}) \cdot \langle \nu, \mathbf{k} | \mathbf{S}_{\ell j} | 0 \rangle, \quad (73)$$

where \mathbf{f}_j is dependent on the interaction type and \mathbf{S}_{ℓ_j} are the ion effective spins which can come both from electronic spin and orbital angular momentum; see Refs. [71, 77] for details. This shows that one needs a net spin on each unit cell in order to excite a response.

The rate is then computed from Fermi's Golden Rule, Eq. (38), which in the case at hand becomes

$$\Gamma(\mathbf{v}) = \int \frac{d^3q}{(2\pi)^3} \sum_{\nu, \mathbf{k}} \left| \sum_{\ell, j} \langle \nu, \mathbf{k} | e^{-i\mathbf{q} \cdot \mathbf{x}_{\ell j}} V_{\ell j}(\mathbf{q}, \mathbf{v}) | 0 \rangle \right|^2 2\pi \delta(E_f - E_i - \omega). \quad (74)$$

B. Target Response to Dark Matter Absorption

In this subsection, we discuss DM absorption in materials, focusing on the case of vector DM and pseudoscalar (axion) DM. For the case of absorption, the energy absorbed is simply the mass, $\omega = m_\chi$, which is much greater than the momentum, $q = m_\chi v$, $\omega \gg q$. This implies one of two possibilities to kinematically allow for DM absorption:

1. an inelastic transition in the target material, implying the presence of a gapped mode having $\omega_q \neq 0$ as $q \rightarrow 0$;
2. an absorption process with two excitations in the final state, where the momentum of the two excitations cancels (to high precision) while the sum of their energies equals m_χ .

It has long been appreciated that new particles, produced in the sun, can be absorbed on target materials via inelastic transitions [99, 100], such as valence electrons in semiconductors making a valence to conduction band transition. More recently, these ideas were applied to vector axion DM absorption on electrons in Xenon [101, 102]. The absorption rate can be related to the complex conductivity via the optical theorem

$$\Gamma_\gamma = -\frac{\text{Im}\Pi(\omega)}{\omega}, \quad (75)$$

where Π is related to the complex conductivity $\hat{\sigma}(\omega)$

$$\Pi(\omega) \approx -i\hat{\sigma}\omega, \quad (76)$$

with Π having transverse and longitudinal polarizations as in Eq. 59. Since $|\mathbf{q}| \ll \omega$, $\Pi_L = \Pi_T \simeq \Pi$. The dark photon absorption rate, per unit target mass, given by

$$\Gamma_{A'} = \frac{1}{\rho_T} \frac{\rho_\chi}{m_\chi} \epsilon_{\text{eff}}^2 \Gamma_\gamma, \quad (77)$$

with ϵ_{eff} (for an isotropic non-magnetic medium) given by Eq. 59. For an anisotropic material, the absorption rate, per unit target mass, is [98]

$$R = -\frac{1}{3} \frac{\rho_\chi}{\rho_T} \sum_{i=1}^3 \epsilon_{\text{eff},i}^2 \frac{\text{Im}\pi_i(q)}{m_{A'}^2}, \quad (78)$$

where π_i are the eigenvalues of the polarization tensor.

The axion absorption rate on electrons can be extracted from Eq. 75 by using the relation with the photon absorption rate [103]:

$$|\mathcal{M}|^2 \approx 3(g_{aee}/2m_e)^2 (m_a/e)^2 |\mathcal{M}_\gamma|^2. \quad (79)$$

Axions can also be absorbed on gapped optical phonons [89]. These modes, similar to electrons in a semiconductor, have a gap at zero momentum transfer, as shown in Fig. 5. Unlike the case of absorption on electrons, where one can make use of the direct axion electron coupling, the interaction goes via the mixing of the phonon with the photon (known as the phonon-polariton), in the presence of an external B -field.

In the second process enumerated above, two modes recoil against each other. In this case, the momentum can be conserved by a cancellation between the two outgoing modes; this cancellation is necessary for acoustic phonons because, for a fixed energy deposition, they have a large amount of momentum in comparison to the DM momentum due to the small speed of sound in comparison to the DM velocity, $c_s \ll v_\chi$:

$$q_{\text{ph}} = \frac{\omega}{c_s} \gg \frac{\omega}{v_\chi}. \quad (80)$$

For example, bosonic DM can be absorbed on free electrons in superconductors by emitting a phonon [104], on two gapless phonons in superfluid helium [92], or on a photon and phonon [105]. All become kinematically possible because of the back-to-back recoil of the two final state excitations. Note that in the cases where only one excitation is produced (*e.g.* electron or optical phonon excitation in semiconductors), momentum is conserved by recoil against the lattice.

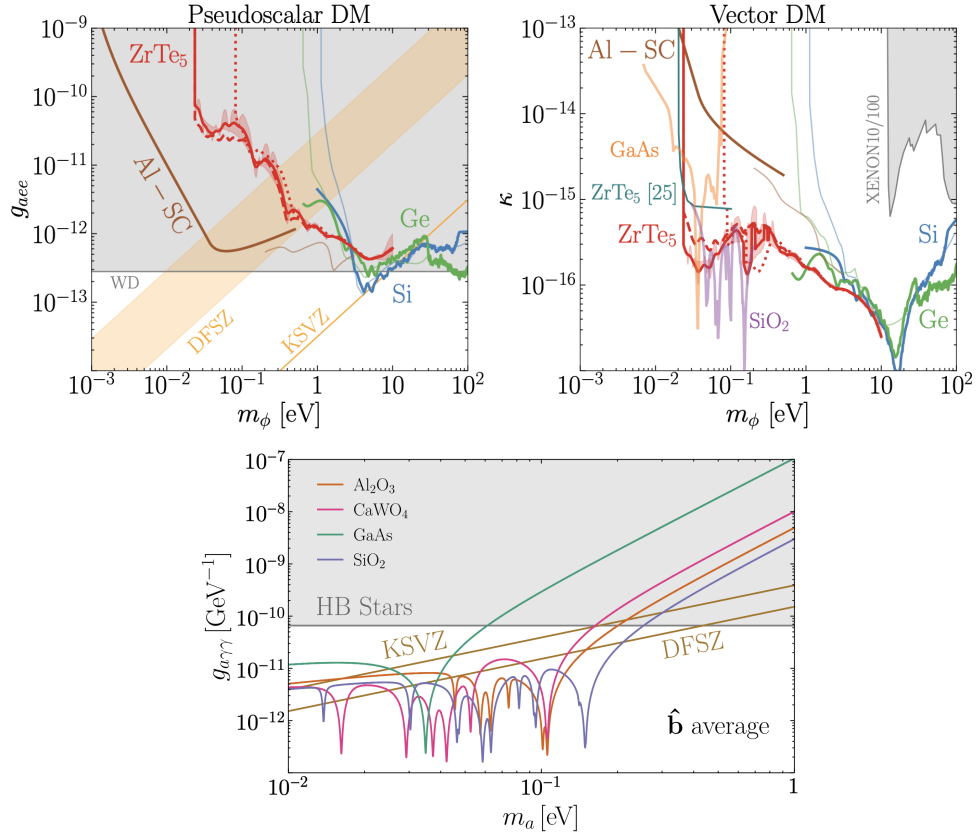


Figure 6. *Upper*: Reach to axion (*left*) and vector (*right*) DM via their electron (*left*) or kinetic mixing (*right*) coupling to the target material, for 1 kg-year exposure. Figures reproduced from Ref. [74]. *Lower*: Reach to axion DM by absorption on phonon-polaritons in a 1T external magnetic field. Figure reproduced from Ref. [89].

A summary plot comparing the reach of axion and dark photon absorption on electrons in semiconductors and superconductors, and on phonon-polaritons in polar crystals, is shown in Fig. 6.

Here, we have chosen to restrict ourselves to particular models whose absorption rate can be simply related to photon interaction rates. One can also pursue an EFT framework for absorption on both electrons [74, 106] and collective modes (phonons [88] and magnons [71]). We direct the reader to these references for further details on more general types of interactions, including DM absorption via electric and magnetic dipoles.

VII. CONCLUSIONS

We have reviewed the development of theories of particle DM of a very low mass, below the traditional WIMP window of ~ 10 GeV but above the mass ~ 1 eV where DM becomes wavelike (*e.g.* axions). Such models are motivated by hidden sector theories, and have rich cosmological and astrophysical dynamics, from self-interactions to impacts on stellar evolution and observational consequences in collider experiments. We have reviewed the astrophysical, cosmological and collider constraints most directly relevant for the model space in terrestrial direct detection experiments.

While 15 years ago, direct detection experiments could not reach the sub-GeV DM mass window, the proposal of hidden sector DM led to an explosion of ideas for direct detection experiments. A subsequent push, in the last 5-10 years, to realize these experiments with research and development gave rise to funded experiments that are actively reaching new theory space. At the present moment, these experimental efforts have not yet covered the best-motivated candidates, such as asymmetric DM, thermal freeze-out DM and DM produced through freeze-in. As these new experiments come to fruition and push to lower cross-sections with better handles on backgrounds and systematic uncertainties, we look forward to the possible uncovering of the Universe's dark side.

ACKNOWLEDGMENTS

I thank Yufeng Du, Osmond Wen, Zhengkang Zhang, and especially Clara Murgui and Tanner Trickle for a careful reading of the manuscript. This work was supported by the U.S. Department of Energy, Office of Science, Quantum Information Science Enabled Discovery (QuantISED) for High Energy Physics (KA2401032), by the Office of High Energy Physics under Award Number DE-SC0011632, by a Simons Investigator Award, and by the Walter Burke Institute for Theoretical Physics.

[1] G. Bertone, D. Hooper, and J. Silk, Particle dark matter: Evidence, candidates and constraints, *Phys. Rept.* **405**, 279 (2005), arXiv:hep-ph/0404175.

- [2] J. Cooley *et al.*, Report of the Topical Group on Particle Dark Matter for Snowmass 2021, (2022), arXiv:2209.07426 [hep-ph].
- [3] C. B. Adams *et al.*, Axion Dark Matter, *Snowmass 2021*, (2022), arXiv:2203.14923 [hep-ex].
- [4] N. Afshordi, P. McDonald, and D. N. Spergel, Primordial black holes as dark matter: The Power spectrum and evaporation of early structures, *Astrophys. J. Lett.* **594**, L71 (2003), arXiv:astro-ph/0302035.
- [5] H. Ramani, T. Trickle, and K. M. Zurek, Observability of Dark Matter Substructure with Pulsar Timing Correlations, *JCAP* **12**, 033, arXiv:2005.03030 [astro-ph.CO].
- [6] K. Van Tilburg, A.-M. Taki, and N. Weiner, Halometry from Astrometry, *JCAP* **07**, 041, arXiv:1804.01991 [astro-ph.CO].
- [7] M. I. Gresham, V. S. H. Lee, and K. M. Zurek, Astrophysical observations of a dark matter-Baryon fifth force, *JCAP* **02**, 048, arXiv:2209.03963 [astro-ph.HE].
- [8] M. Battaglieri *et al.*, US Cosmic Visions: New Ideas in Dark Matter 2017: Community Report, in *U.S. Cosmic Visions: New Ideas in Dark Matter* (2017) arXiv:1707.04591 [hep-ph].
- [9] E. O. Nadler *et al.* (DES), Milky Way Satellite Census. III. Constraints on Dark Matter Properties from Observations of Milky Way Satellite Galaxies, *Phys. Rev. Lett.* **126**, 091101 (2021), arXiv:2008.00022 [astro-ph.CO].
- [10] M. J. Strassler and K. M. Zurek, Echoes of a hidden valley at hadron colliders, *Phys. Lett. B* **651**, 374 (2007), arXiv:hep-ph/0604261.
- [11] M. J. Strassler and K. M. Zurek, Discovering the Higgs through highly-displaced vertices, *Phys. Lett. B* **661**, 263 (2008), arXiv:hep-ph/0605193.
- [12] C. Boehm and P. Fayet, Scalar dark matter candidates, *Nucl. Phys. B* **683**, 219 (2004), arXiv:hep-ph/0305261.
- [13] M. Pospelov, A. Ritz, and M. B. Voloshin, Secluded WIMP Dark Matter, *Phys. Lett. B* **662**, 53 (2008), arXiv:0711.4866 [hep-ph].
- [14] M. Pospelov and A. Ritz, Astrophysical Signatures of Secluded Dark Matter, *Phys. Lett. B* **671**, 391 (2009), arXiv:0810.1502 [hep-ph].
- [15] D. E. Kaplan, M. A. Luty, and K. M. Zurek, Asymmetric Dark Matter, *Phys. Rev. D* **79**, 115016 (2009), arXiv:0901.4117 [hep-ph].

- [16] K. M. Zurek, Asymmetric Dark Matter: Theories, Signatures, and Constraints, *Phys. Rept.* **537**, 91 (2014), arXiv:1308.0338 [hep-ph].
- [17] D. E. Kaplan, G. Z. Krnjaic, K. R. Rehermann, and C. M. Wells, Atomic Dark Matter, *JCAP* **05**, 021, arXiv:0909.0753 [hep-ph].
- [18] G. D. Kribs, T. S. Roy, J. Terning, and K. M. Zurek, Quirky Composite Dark Matter, *Phys. Rev. D* **81**, 095001 (2010), arXiv:0909.2034 [hep-ph].
- [19] K. K. Boddy, J. L. Feng, M. Kaplinghat, and T. M. P. Tait, Self-Interacting Dark Matter from a Non-Abelian Hidden Sector, *Phys. Rev. D* **89**, 115017 (2014), arXiv:1402.3629 [hep-ph].
- [20] J. L. Feng and J. Kumar, The WIMPless Miracle: Dark-Matter Particles without Weak-Scale Masses or Weak Interactions, *Phys. Rev. Lett.* **101**, 231301 (2008), arXiv:0803.4196 [hep-ph].
- [21] Y. Hochberg, E. Kuflik, H. Murayama, T. Volansky, and J. G. Wacker, Model for Thermal Relic Dark Matter of Strongly Interacting Massive Particles, *Phys. Rev. Lett.* **115**, 021301 (2015), arXiv:1411.3727 [hep-ph].
- [22] B. Holdom, Two U(1)'s and Epsilon Charge Shifts, *Phys. Lett. B* **166**, 196 (1986).
- [23] D. Hooper and K. M. Zurek, A Natural Supersymmetric Model with MeV Dark Matter, *Phys. Rev. D* **77**, 087302 (2008), arXiv:0801.3686 [hep-ph].
- [24] S. Knapen, T. Lin, and K. M. Zurek, Light Dark Matter: Models and Constraints, *Phys. Rev. D* **96**, 115021 (2017), arXiv:1709.07882 [hep-ph].
- [25] B. Patt and F. Wilczek, Higgs-field portal into hidden sectors, (2006), arXiv:hep-ph/0605188.
- [26] C. Murgui and K. M. Zurek, Dark unification: A UV-complete theory of asymmetric dark matter, *Phys. Rev. D* **105**, 095002 (2022), arXiv:2112.08374 [hep-ph].
- [27] T. Cohen, D. J. Phalen, A. Pierce, and K. M. Zurek, Asymmetric Dark Matter from a GeV Hidden Sector, *Phys. Rev. D* **82**, 056001 (2010), arXiv:1005.1655 [hep-ph].
- [28] S. Galli, F. Iocco, G. Bertone, and A. Melchiorri, Updated CMB constraints on Dark Matter annihilation cross-sections, *Phys. Rev. D* **84**, 027302 (2011), arXiv:1106.1528 [astro-ph.CO].
- [29] D. P. Finkbeiner, S. Galli, T. Lin, and T. R. Slatyer, Searching for Dark Matter in the CMB: A Compact Parameterization of Energy Injection from New Physics, *Phys. Rev. D* **85**, 043522 (2012), arXiv:1109.6322 [astro-ph.CO].
- [30] T. Lin, H.-B. Yu, and K. M. Zurek, On Symmetric and Asymmetric Light Dark Matter, *Phys. Rev. D* **85**, 063503 (2012), arXiv:1111.0293 [hep-ph].

- [31] M. S. Madhavacheril, N. Sehgal, and T. R. Slatyer, Current Dark Matter Annihilation Constraints from CMB and Low-Redshift Data, *Phys. Rev. D* **89**, 103508 (2014), arXiv:1310.3815 [astro-ph.CO].
- [32] C. Boehm, P. Fayet, and J. Silk, Light and heavy dark matter particles, *Phys. Rev. D* **69**, 101302 (2004), arXiv:hep-ph/0311143.
- [33] D. Hooper, M. Kaplinghat, L. E. Strigari, and K. M. Zurek, MeV Dark Matter and Small Scale Structure, *Phys. Rev. D* **76**, 103515 (2007), arXiv:0704.2558 [astro-ph].
- [34] M. L. Graesser, I. M. Shoemaker, and L. Vecchi, Asymmetric WIMP dark matter, *JHEP* **10**, 110, arXiv:1103.2771 [hep-ph].
- [35] L. J. Hall, K. Jedamzik, J. March-Russell, and S. M. West, Freeze-In Production of FIMP Dark Matter, *JHEP* **03**, 080, arXiv:0911.1120 [hep-ph].
- [36] C. Dvorkin, T. Lin, and K. Schutz, Making dark matter out of light: freeze-in from plasma effects, *Phys. Rev. D* **99**, 115009 (2019), [Erratum: *Phys.Rev.D* 105, 119901 (2022)], arXiv:1902.08623 [hep-ph].
- [37] X. Chu, T. Hambye, and M. H. G. Tytgat, The Four Basic Ways of Creating Dark Matter Through a Portal, *JCAP* **05**, 034, arXiv:1112.0493 [hep-ph].
- [38] Y. Hochberg, E. Kuflik, T. Volansky, and J. G. Wacker, Mechanism for Thermal Relic Dark Matter of Strongly Interacting Massive Particles, *Phys. Rev. Lett.* **113**, 171301 (2014), arXiv:1402.5143 [hep-ph].
- [39] E. Kuflik, M. Perelstein, N. R.-L. Lorier, and Y.-D. Tsai, Phenomenology of ELDER Dark Matter, *JHEP* **08**, 078, arXiv:1706.05381 [hep-ph].
- [40] E. D. Carlson, M. E. Machacek, and L. J. Hall, Self-interacting dark matter, *Astrophys. J.* **398**, 43 (1992).
- [41] A. A. de Laix, R. J. Scherrer, and R. K. Schaefer, Constraints of selfinteracting dark matter, *Astrophys. J.* **452**, 495 (1995), arXiv:astro-ph/9502087.
- [42] E. Kuflik, M. Perelstein, N. R.-L. Lorier, and Y.-D. Tsai, Elastically Decoupling Dark Matter, *Phys. Rev. Lett.* **116**, 221302 (2016), arXiv:1512.04545 [hep-ph].
- [43] T.-H. Yeh, K. A. Olive, and B. D. Fields, The impact of new $d(p, \gamma)3$ rates on Big Bang Nucleosynthesis, *JCAP* **03**, 046, arXiv:2011.13874 [astro-ph.CO].

- [44] T.-H. Yeh, J. Shelton, K. A. Olive, and B. D. Fields, Probing physics beyond the standard model: limits from BBN and the CMB independently and combined, *JCAP* **10**, 046, arXiv:2207.13133 [astro-ph.CO].
- [45] W. Enzi *et al.*, Joint constraints on thermal relic dark matter from strong gravitational lensing, the Ly α forest, and Milky Way satellites, *Mon. Not. Roy. Astron. Soc.* **506**, 5848 (2021), arXiv:2010.13802 [astro-ph.CO].
- [46] A. E. Nelson and J. Scholtz, Dark Light, Dark Matter and the Misalignment Mechanism, *Phys. Rev. D* **84**, 103501 (2011), arXiv:1105.2812 [hep-ph].
- [47] P. W. Graham, J. Mardon, and S. Rajendran, Vector Dark Matter from Inflationary Fluctuations, *Phys. Rev. D* **93**, 103520 (2016), arXiv:1504.02102 [hep-ph].
- [48] S. Tulin and H.-B. Yu, Dark Matter Self-interactions and Small Scale Structure, *Phys. Rept.* **730**, 1 (2018), arXiv:1705.02358 [hep-ph].
- [49] Y. Hochberg, M. Pyle, Y. Zhao, and K. M. Zurek, Detecting Superlight Dark Matter with Fermi-Degenerate Materials, *JHEP* **08**, 057, arXiv:1512.04533 [hep-ph].
- [50] S. Knapen, T. Lin, M. Pyle, and K. M. Zurek, Detection of Light Dark Matter With Optical Phonons in Polar Materials, *Phys. Lett. B* **785**, 386 (2018), arXiv:1712.06598 [hep-ph].
- [51] G. G. Raffelt, *Stars as laboratories for fundamental physics: The astrophysics of neutrinos, axions, and other weakly interacting particles* (1996).
- [52] J. H. Chang, R. Essig, and S. D. McDermott, Supernova 1987A Constraints on Sub-GeV Dark Sectors, Millicharged Particles, the QCD Axion, and an Axion-like Particle, *JHEP* **09**, 051, arXiv:1803.00993 [hep-ph].
- [53] M. Baryakhtar, J. Bramante, S. W. Li, T. Linden, and N. Raj, Dark Kinetic Heating of Neutron Stars and An Infrared Window On WIMPs, SIMPs, and Pure Higgsinos, *Phys. Rev. Lett.* **119**, 131801 (2017), arXiv:1704.01577 [hep-ph].
- [54] M. Taoso, F. Iocco, G. Meynet, G. Bertone, and P. Eggenberger, Effect of low mass dark matter particles on the Sun, *Phys. Rev. D* **82**, 083509 (2010), arXiv:1005.5711 [astro-ph.CO].
- [55] A. R. Zentner and A. P. Hearin, Asymmetric Dark Matter May Alter the Evolution of Low-mass Stars and Brown Dwarfs, *Phys. Rev. D* **84**, 101302 (2011), arXiv:1110.5919 [astro-ph.CO].

- [56] S. C. Leung, M. C. Chu, L. M. Lin, and K. W. Wong, Dark-matter admixed white dwarfs, *Phys. Rev. D* **87**, 123506 (2013), arXiv:1305.6142 [astro-ph.CO].
- [57] P. W. Graham, R. Janish, V. Narayan, S. Rajendran, and P. Riggins, White Dwarfs as Dark Matter Detectors, *Phys. Rev. D* **98**, 115027 (2018), arXiv:1805.07381 [hep-ph].
- [58] A. Joglekar, N. Raj, P. Tanedo, and H.-B. Yu, Dark kinetic heating of neutron stars from contact interactions with relativistic targets, *Phys. Rev. D* **102**, 123002 (2020), arXiv:2004.09539 [hep-ph].
- [59] E. Izaguirre, G. Krnjaic, P. Schuster, and N. Toro, New Electron Beam-Dump Experiments to Search for MeV to few-GeV Dark Matter, *Phys. Rev. D* **88**, 114015 (2013), arXiv:1307.6554 [hep-ph].
- [60] E. Izaguirre, G. Krnjaic, P. Schuster, and N. Toro, Testing GeV-Scale Dark Matter with Fixed-Target Missing Momentum Experiments, *Phys. Rev. D* **91**, 094026 (2015), arXiv:1411.1404 [hep-ph].
- [61] J. D. Bjorken, R. Essig, P. Schuster, and N. Toro, New Fixed-Target Experiments to Search for Dark Gauge Forces, *Phys. Rev. D* **80**, 075018 (2009), arXiv:0906.0580 [hep-ph].
- [62] S. Andreas, C. Niebuhr, and A. Ringwald, New Limits on Hidden Photons from Past Electron Beam Dumps, *Phys. Rev. D* **86**, 095019 (2012), arXiv:1209.6083 [hep-ph].
- [63] T. Trickle, Z. Zhang, K. M. Zurek, K. Inzani, and S. M. Griffin, Multi-Channel Direct Detection of Light Dark Matter: Theoretical Framework, *JHEP* **03**, 036, arXiv:1910.08092 [hep-ph].
- [64] R. Essig, J. Mardon, and T. Volansky, Direct Detection of Sub-GeV Dark Matter, *Phys. Rev. D* **85**, 076007 (2012), arXiv:1108.5383 [hep-ph].
- [65] P. W. Graham, D. E. Kaplan, S. Rajendran, and M. T. Walters, Semiconductor Probes of Light Dark Matter, *Phys. Dark Univ.* **1**, 32 (2012), arXiv:1203.2531 [hep-ph].
- [66] R. Essig, M. Fernandez-Serra, J. Mardon, A. Soto, T. Volansky, and T.-T. Yu, Direct Detection of sub-GeV Dark Matter with Semiconductor Targets, *JHEP* **05**, 046, arXiv:1509.01598 [hep-ph].
- [67] Y. Hochberg, Y. Kahn, M. Lisanti, K. M. Zurek, A. G. Grushin, R. Ilan, S. M. Griffin, Z.-F. Liu, S. F. Weber, and J. B. Neaton, Detection of sub-MeV Dark Matter with Three-Dimensional Dirac Materials, *Phys. Rev. D* **97**, 015004 (2018), arXiv:1708.08929 [hep-ph].

- [68] R. Essig, J. Mardon, O. Slone, and T. Volansky, Detection of sub-GeV Dark Matter and Solar Neutrinos via Chemical-Bond Breaking, *Phys. Rev. D* **95**, 056011 (2017), arXiv:1608.02940 [hep-ph].
- [69] S. M. Griffin, K. Inzani, T. Trickle, Z. Zhang, and K. M. Zurek, Multichannel direct detection of light dark matter: Target comparison, *Phys. Rev. D* **101**, 055004 (2020), arXiv:1910.10716 [hep-ph].
- [70] R. Anthony-Petersen *et al.*, A Stress Induced Source of Phonon Bursts and Quasiparticle Poisoning, (2022), arXiv:2208.02790 [physics.ins-det].
- [71] T. Trickle, Z. Zhang, and K. M. Zurek, Detecting Light Dark Matter with Magnons, *Phys. Rev. Lett.* **124**, 201801 (2020), arXiv:1905.13744 [hep-ph].
- [72] C. Blanco, J. I. Collar, Y. Kahn, and B. Lillard, Dark Matter-Electron Scattering from Aromatic Organic Targets, *Phys. Rev. D* **101**, 056001 (2020), arXiv:1912.02822 [hep-ph].
- [73] Y. Hochberg, Y. Zhao, and K. M. Zurek, Superconducting Detectors for Superlight Dark Matter, *Phys. Rev. Lett.* **116**, 011301 (2016), arXiv:1504.07237 [hep-ph].
- [74] H.-Y. Chen, A. Mitridate, T. Trickle, Z. Zhang, M. Bernardi, and K. M. Zurek, Dark matter direct detection in materials with spin-orbit coupling, *Phys. Rev. D* **106**, 015024 (2022), arXiv:2202.11716 [hep-ph].
- [75] Y. Hochberg, Y. Kahn, N. Kurinsky, B. V. Lehmann, T. C. Yu, and K. K. Berggren, Determining Dark-Matter–Electron Scattering Rates from the Dielectric Function, *Phys. Rev. Lett.* **127**, 151802 (2021), arXiv:2101.08263 [hep-ph].
- [76] P. Du, D. Egaña Ugrinovic, R. Essig, and M. Sholapurkar, Doped Semiconductor Devices for sub-MeV Dark Matter Detection, (2022), arXiv:2212.04504 [hep-ph].
- [77] T. Trickle, Z. Zhang, and K. M. Zurek, Effective field theory of dark matter direct detection with collective excitations, *Phys. Rev. D* **105**, 015001 (2022), arXiv:2009.13534 [hep-ph].
- [78] S. M. Griffin, K. Inzani, T. Trickle, Z. Zhang, and K. M. Zurek, Extended calculation of dark matter-electron scattering in crystal targets, *Phys. Rev. D* **104**, 095015 (2021), arXiv:2105.05253 [hep-ph].
- [79] S. K. Lee, M. Lisanti, S. Mishra-Sharma, and B. R. Safdi, Modulation Effects in Dark Matter-Electron Scattering Experiments, *Phys. Rev. D* **92**, 083517 (2015), arXiv:1508.07361 [hep-ph].

- [80] Y. Hochberg, Y. Kahn, M. Lisanti, C. G. Tully, and K. M. Zurek, Directional detection of dark matter with two-dimensional targets, *Phys. Lett. B* **772**, 239 (2017), arXiv:1606.08849 [hep-ph].
- [81] C. E. Dreyer, R. Essig, M. Fernandez-Serra, A. Singal, and C. Zhen, Fully ab-initio all-electron calculation of dark matter–electron scattering in crystals with evaluation of systematic uncertainties, (2023), arXiv:2306.14944 [hep-ph].
- [82] T. Trickle, Extended calculation of electronic excitations for direct detection of dark matter, *Phys. Rev. D* **107**, 035035 (2023), arXiv:2210.14917 [hep-ph].
- [83] S. Knapen, J. Kozaczuk, and T. Lin, python package for dark matter scattering in dielectric targets, *Phys. Rev. D* **105**, 015014 (2022), arXiv:2104.12786 [hep-ph].
- [84] S. Knapen, J. Kozaczuk, and T. Lin, Dark matter-electron scattering in dielectrics, *Phys. Rev. D* **104**, 015031 (2021), arXiv:2101.08275 [hep-ph].
- [85] Y. Hochberg, B. V. Lehmann, I. Charaev, J. Chiles, M. Colangelo, S. W. Nam, and K. K. Berggren, New constraints on dark matter from superconducting nanowires, *Phys. Rev. D* **106**, 112005 (2022), arXiv:2110.01586 [hep-ph].
- [86] R. Essig *et al.*, Snowmass2021 Cosmic Frontier: The landscape of low-threshold dark matter direct detection in the next decade, in *Snowmass 2021* (2022) arXiv:2203.08297 [hep-ph].
- [87] S. Griffin, S. Knapen, T. Lin, and K. M. Zurek, Directional Detection of Light Dark Matter with Polar Materials, *Phys. Rev. D* **98**, 115034 (2018), arXiv:1807.10291 [hep-ph].
- [88] A. Mitridate, K. Pardo, T. Trickle, and K. M. Zurek, Effective Field Theory for Dark Matter Absorption on Single Phonons, (2023), arXiv:2308.06314 [hep-ph].
- [89] A. Mitridate, T. Trickle, Z. Zhang, and K. M. Zurek, Detectability of Axion Dark Matter with Phonon Polaritons and Magnons, *Phys. Rev. D* **102**, 095005 (2020), arXiv:2005.10256 [hep-ph].
- [90] N. Crescini *et al.* (QUAX), Axion search with a quantum-limited ferromagnetic haloscope, *Phys. Rev. Lett.* **124**, 171801 (2020), arXiv:2001.08940 [hep-ex].
- [91] K. Schutz and K. M. Zurek, Detectability of Light Dark Matter with Superfluid Helium, *Phys. Rev. Lett.* **117**, 121302 (2016), arXiv:1604.08206 [hep-ph].
- [92] S. Knapen, T. Lin, and K. M. Zurek, Light Dark Matter in Superfluid Helium: Detection with Multi-excitation Production, *Phys. Rev. D* **95**, 056019 (2017), arXiv:1611.06228 [hep-ph].

- [93] A. Caputo, A. Esposito, and A. D. Polosa, Light Dark Matter and Superfluid He-4 from EFT, *J. Phys. Conf. Ser.* **1468**, 012060 (2020), arXiv:1911.07867 [hep-ph].
- [94] F. Acanfora, A. Esposito, and A. D. Polosa, Sub-GeV Dark Matter in Superfluid He-4: an Effective Theory Approach, *Eur. Phys. J. C* **79**, 549 (2019), arXiv:1902.02361 [hep-ph].
- [95] B. Campbell-Deem, S. Knapen, T. Lin, and E. Villarama, Dark matter direct detection from the single phonon to the nuclear recoil regime, *Phys. Rev. D* **106**, 036019 (2022), arXiv:2205.02250 [hep-ph].
- [96] T. Lin, C.-H. Shen, M. Sholapurkar, and E. Villarama, Anharmonic effects in nuclear recoils from sub-GeV dark matter, (2023), arXiv:2309.10839 [hep-ph].
- [97] G. Baym, D. H. Beck, J. P. Filippini, C. J. Pethick, and J. Shelton, Searching for low mass dark matter via phonon creation in superfluid ^4He , *Phys. Rev. D* **102**, 035014 (2020), [Erratum: *Phys.Rev.D* 104, 019901 (2021)], arXiv:2005.08824 [hep-ph].
- [98] A. Coskuner, A. Mitridate, A. Olivares, and K. M. Zurek, Directional Dark Matter Detection in Anisotropic Dirac Materials, *Phys. Rev. D* **103**, 016006 (2021), arXiv:1909.09170 [hep-ph].
- [99] S. Dimopoulos, G. D. Starkman, and B. W. Lynn, Atomic Enhancements in the Detection of Axions, *Mod. Phys. Lett. A* **1**, 491 (1986).
- [100] G. Gelmini, S. P. Ahlen, F. T. Avignone, R. L. Brodzinski, S. Dimopoulos, A. K. Drukier, B. W. Lynn, D. N. Spergel, and G. D. Starkman, BOUNDS FROM DIRECT SEARCH OF GALACTIC COLD DARK MATTER AND SOLAR AXIONS FROM A GE SPECTROMETER (1987).
- [101] M. Pospelov, A. Ritz, and M. B. Voloshin, Bosonic super-WIMPs as keV-scale dark matter, *Phys. Rev. D* **78**, 115012 (2008), arXiv:0807.3279 [hep-ph].
- [102] H. An, M. Pospelov, J. Pradler, and A. Ritz, Direct Detection Constraints on Dark Photon Dark Matter, *Phys. Lett. B* **747**, 331 (2015), arXiv:1412.8378 [hep-ph].
- [103] Y. Hochberg, T. Lin, and K. M. Zurek, Detecting Ultralight Bosonic Dark Matter via Absorption in Superconductors, *Phys. Rev. D* **94**, 015019 (2016), arXiv:1604.06800 [hep-ph].
- [104] Y. Hochberg, T. Lin, and K. M. Zurek, Absorption of light dark matter in semiconductors, *Phys. Rev. D* **95**, 023013 (2017), arXiv:1608.01994 [hep-ph].
- [105] C. Murgui, Y. Wang, and K. M. Zurek, Axion Detection with Optomechanical Cavities, (2022), arXiv:2211.08432 [hep-ph].

- [106] G. Krnjaic and T. Trickle, Absorption of vector dark matter beyond kinetic mixing, *Phys. Rev. D* **108**, 015024 (2023), arXiv:2303.11344 [hep-ph].